https://doi.org/10.5194/egusphere-2022-804
Preprint. Discussion started: 24 August 2022

Deglacial and Holocene sea ice and climate dynamics at the Western Antarctic Peninsula

Maria-Elena Vorrath[1], Juliane Müller[2,3,4], Paola Cárdenas[5], Sebastian Mieruch[2], Oliver Esper[2], Thomas Opel[2], Lester Lembke-Jene[2], Johan Etourneau[6,7], Andrea Vieth-Hillebrand[8], Niko Lahajnar[1], Carina B. Lange[5,9,10,11], Amy Leventer[12], Dimitris Evangelinos[7,13], Carlota Escutia[14], Gesine Mollenhauer[2,3]

[1]University Hamburg, Institute for Geology, Hamburg, Germany

[2]Alfred Wegener Institute, Helmholtz Centre for Polar and Marine Research, Bremerhaven, Germany

[3]MARUM – Center for Marine Environmental Sciences, University of Bremen, Germany

[4]Department of Geosciences, University of Bremen, Germany

[5]Centro de Investigación Dinámica de Ecosistemas Marinos de Altas Latitudes (IDEAL), Universidad Austral de Chile, Valdivia, Chile

[6]EPHE/PSL Research University, France

[7]UMR 5805 EPOC, CNRS, Université de Bordeaux, France

[8]Helmholtz Centre Potsdam GFZ German Research Centre for Geosciences, Potsdam, Germany

[9]Centro Oceanográfico COPAS Sur-Austral/COPAS-Coastal, Universidad de Concepción, Chile

[10]Departamento de Oceanografía, Universidad de Concepción, Chile

[11]Scripps Institution of Oceanography, La Jolla, CA 92037, USA

[12]Department of Geology, Colgate University, New York, USA

[13]Departament de Dinàmica de la Terra i de l'Oceà, Universitat de Barcelona, Spain

[14]Instituto Andaluz de Ciencia de la tierra, CSIC-Univ. de Granada, Spain

Correspondence to: Juliane Müller, juliane.mueller@awi.de

Abstract

The reconstruction of past sea ice distribution in the Southern Ocean is crucial for an improved understanding of ice-ocean-atmosphere feedbacks and the evaluation of Earth system and Antarctic ice sheet models. The Western Antarctic Peninsula (WAP) is experiencing rapid warming and the associated decrease in sea ice cover contrasts the trend of growing sea ice extent in eastern Antarctica. To reveal the long-term sea ice history at the WAP under

https://doi.org/10.5194/egusphere-2022-804
Preprint. Discussion started: 24 August 2022

changing climate conditions we examined a marine sediment core from the eastern basin of the Bransfield Strait covering the last Deglacial and the Holocene. For sea ice reconstructions, we focused on the specific sea ice biomarker lipid $IPSO_{25}$, a highly branched isoprenoid (HBI), and sea ice diatoms, whereas a phytoplankton-derived HBI triene ($C_{25:3}$) and open ocean diatom assemblages reflect predominantly ice-free conditions. We further reconstruct ocean temperatures using glycerol dialkyl glycerol tetraether (GDGTs) and diatom assemblages, and compare our sea ice and temperature records with published marine sediment and ice core data. Our results document a retreat of the WAP ice shelf at 13.9 ka BP (before present). Maximum sea ice cover is observed during the Antarctic Cold Reversal, while a still extended but variable sea ice coverage characterized the core site during the early Holocene. An overall decreasing sea ice trend throughout the Middle Holocene is accompanied by a successive ocean warming and increasing phytoplankton productivity. The Late Holocene is characterized by unstable (winter) sea ice conditions and a further sea ice decline until 0.5 ka BP.

Key Words: Western Antarctic Peninsula, Holocene, sea ice cover, $IPSO_{25}$, highly branched isoprenoids, diatoms

1 Introduction

Sea ice significantly affects the global climate system through its impact on the atmosphere-ocean exchange of heat and gas, physical and chemical properties of the water masses, ocean circulation, primary production and biogeochemical cycles (Chisholm, 2000; Vancoppenolle et al., 2013). Sea ice cover limits evaporation, affects precipitation and increases the reflection of solar radiation due to a high albedo (Allison et al., 1982; Butterworth and Miller, 2016; Turner et al., 2017). When sea ice forms, cold and dense brines develop contributing to the formation of intermediate and deep waters (Nicholls et al., 2009). Importantly, these dense water masses prevent warm currents from reaching the continental slope where they stimulate the basal melt of Antarctic ice shelves with implications for the stability of ice sheets and eventually global sea level (Cook et al., 2016; Escutia et al., 2019; Etourneau et al., 2019; Hellmer et al., 2012; Huss and Farinotti, 2014). During the spring season, sea ice melting stimulates marine primary production by seeding algal cells, the release of nutrients and by promoting ocean stratification and a shallow mixed layer depth (Arrigo et al., 1997; Vernet et al., 2008). In addition, nutrient supply can be locally enhanced by increasing wind-driven upwelling activity along the sea ice edge, thus triggering phytoplankton blooms (Alexander and Niebauer, 1981). Enhanced carbon fixation through this nutrient-stimulated biological pump hence leads to an increase of biological material transport and organic carbon export to the ocean floor, thus contributing to lower surface pCO_2 (Kim et al., 2004; Schofield et al., 2018; Wefer et al., 1988).

Since satellite based sea-ice data became available in 1979, fast and profound changes have been observed globally due to anthropogenic global warming (IPCC, 2021). The Western Antarctic Peninsula (WAP), in particular, is

https://doi.org/10.5194/egusphere-2022-804
Preprint. Discussion started: 24 August 2022

experiencing a rapid warming of the atmosphere (Vaughan et al., 2003) and the ocean (Cook et al., 2016). This is accompanied by rapidly retreating glaciers and ice shelves (Cook et al., 2016; Rignot et al., 2019) and by significant loss of sea ice cover in the adjacent seas (Parkinson and Cavalieri, 2012).

For an assessment of the region's past sensitivity to climate change, the deglacial and Holocene climate history of the Antarctic Peninsula (AP) has been studied extensively. The Deglacial, the transition from the Last Glacial Maximum (LGM, Clark et al., 2012) to the Holocene, is characterized by a rapid warming punctuated by a distinct cold event, the so-called Antarctic Cold Reversal (ACR) from 14.7 ka to 13 ka BP (EPICA Community Members, 2004; Mulvaney et al., 2012; Pedro et al., 2016). This drastic cooling of both atmosphere and ocean temperatures is recorded by stable isotopes in Antarctic ice cores and marine sediments (Blunier and Brook, 2001; Domack et al., 2001; Jouzel et al., 1995; Morigi et al., 2003; Stenni et al., 2001). From the Deglacial towards the Middle Holocene, the Antarctic Peninsula Ice Sheet retreated rapidly from the outer shelf to its modern configuration with heavy melt water discharge (Bentley et al., 2014). Several syntheses of Holocene climate reflected in marine and lake sediment cores reveal that the timing of both hydrological and environmental changes is highly variable at the WAP (Allen et al., 2010; Ingólfsson et al., 2003; Minzoni et al., 2015; Roseby et al., 2022; Sjunneskog and Taylor, 2002; Totten et al., 2022). The ice-core records from James Ross Island (JRI) at the northeastern tip of the AP shows a pronounced warming between about 12 and 11 ka BP followed by a cooling trend until about 9 ka BP and stable temperatures until 2.5 ka BP. Late Holocene cooling was reversed since 0.6 ka BP (Mulvaney et al., 2012). An overall consensus is that ocean temperature in the WAP was, in comparison to the Deglacial or the Late Holocene, warmer during the Early and Middle Holocene Optimum, i.e. between 12 ka and 4 ka BP. In contrast, the Late Holocene shows many different climate patterns around the AP, including a continuous Neoglacial cooling (Etourneau et al., 2013) whereas other records resolve warmer and colder phases such as the Medieval Climate Anomaly and/or the Little Ice Age (Bentley et al., 2009).

Knowledge of past sea ice variability is crucial for modelling climate feedbacks impacting the Antarctic ice sheet stability since the LGM (Crosta et al., 2022). For periods beyond the satellite era, sea-ice knowledge is based on proxies from marine sediments and ice cores (*e.g.* Bracegirdle et al., 2015, 2019; Crosta et al., 2022; Escutia et al., 2019; Thomas et al., 2019). Models, however, often fail to reproduce seasonal sea ice cycles for both glacial and interglacial periods and often disagree with geological proxies (Roche et al., 2012). Ice-core based sea ice reconstructions for the LGM are primarily based on the concentrations of sea salt sodium (WAIS Divide Project Members, 2015). However, since sea-salt aerosols might be overprinted by the highly variable wind direction and meteorological conditions in Antarctica and thus not reflect regional sea ice conditions (Thomas et al., 2019). Although marine sediments mostly have a lower temporal resolution than ice cores, they can resolve regional and/or large-scale changes in sea ice conditions as well as sea surface and subsurface ocean temperature, primary productivity and marine ecology (Hillaire-Marcel and de Vernal, 2007). In addition to commonly used geochemical, lithological and microfossil proxies (*e.g.* ice rafted debris (IRD), diatom assemblages, total organic carbon), new approaches focus on specific organic biomarkers - highly branched isoprenoids (HBIs) - as reliable proxies to distinguish between open marine and sea ice covered environments. The diunsaturated HBI $IPSO_{25}$ (Ice Proxy for the Southern Ocean, $C_{25:2}$, Belt et al., 2016; Massé et al., 2011) has already been applied for Antarctic sea ice reconstructions (*e.g.* Barbara et al., 2013; Denis et al., 2010; Etourneau et al., 2013). Following the PIP_{25} approach for the Arctic (Müller et al., 2011), $IPSO_{25}$ has been combined with HBI trienes and/or sterols to determine the phytoplankton-$IPSO_{25}$ sea ice index called $PIPSO_{25}$ (Vorrath et al., 2019), which has been successfully evaluated with recent sea ice concentrations (Lamping et al., 2021), over periods of the industrial era (Vorrath et al., 2020) and has been used in paleo sea ice studies from the Amundsen Sea (Lamping et al., 2020). Hence, the combination to these new molecular proxies with the classical proxies offer a unique opportunity to robustly reconstruct past sea ice at the WAP.

Here, we present a marine sediment record covering the past 13.9 ka BP to reconstruct Deglacial and Holocene environmental conditions at the WAP. Our study is based on a multiproxy approach focusing on the sea ice biomarker $IPSO_{25}$, a marine phytoplankton biomarker (HBI triene), and on glycerol dialkyl glycerol tetraether lipids (GDGTs) for subsurface ocean temperatures (SOT). Additional information about the probability of winter sea ice (WSI) and summer sea surface temperature (SSST) comes from diatom assemblages using transfer functions. We discuss and compare our proxy results with other marine sediment and ice core records spanning the Holocene providing further insight into environmental dynamics across the Deglacial and the Holocene.

2 Material and Methods

2.1 Study Area

The Bransfield Strait is located between the WAP and the South Shetland Islands (SSI) (Fig. 1a). Within this area, a shallow shelf and deeper depressions characterize the Bransfield Basin with water depths exceeding 2000 m (Fig. 1b). The shelf area was affected by intense ice sheet dynamics during the last glaciation (Canals and Amblas, 2016b; Ingólfsson et al., 2003) leaving ice sheet grounding lines and glacial troughs on the sea floor (Canals et al., 2016; Canals and Amblas, 2016a). The Bransfield Basin is influenced by complex oceanic current systems, which are not fully constrained because three different water masses enter the basin from the east and west (Moffat and Meredith, 2018; Sangrà et al., 2011) and their mixing is not well understood. The cold (< 0° C) and relatively salty Weddell Sea Water (WSW) enters from the east, flows alongshore the peninsula and fills the basin below 150 m

https://doi.org/10.5194/egusphere-2022-804
Preprint. Discussion started: 24 August 2022

surface. The WSW is also observed at greater depths (200-600 m) north of the SSI and at Elephant Island due to wind driven modulation (Meijers et al., 2016). In the western part of the Bransfield Strait, the WSW mixes with a second water mass, the Bellingshausen Sea Water (BSW) (Collares et al., 2018), which is a branch of the Antarctic Circumpolar Current (ACC). It conveys well-stratified, fresh and warmer (> 0°C) surface water (Sangrà et al., 2011). A third water mass originating from the Circumpolar Deep Water (CDW) is present between 200 m and 550 m (Sangrà et al., 2017). BSW and CDW flow eastward along the SSI, turn around and flow westward at the northern tip of the islands (Sangrà et al., 2011). BSW forms the subsurface Bransfield front with the CDW at depth and the surface Peninsula Front (PF) with the WSW, parallel to the Antarctic mainland (Sangrà et al., 2011, 2017). The interplay of currents leads to a stratification of the water column of the upper 20 m in summer, with a steep temperature gradient in the first 100 m below sea surface. This can be observed in CTD profiles in the Bransfield Basin that show a dominance of WSW below 200 m (see Fig. 1c and Sangrà et al., 2011). The eddy system at the Peninsula Front is assumed to play a key role for mixing and upwelling of the different surface and subsurface water masses (Sangrà et al., 2011; Zhou et al., 2002), while several glaciers from the WAP influence coastal surface water due to meltwater discharge and also transport dense bottom waters to the Bransfield Basin (Meredith et al., 2018).

Primary production is mainly driven by mixing of water masses at the fronts (Gonçalves-Araujo et al., 2015), mixed layer depth and upwelling (Sangrà et al., 2011), sea ice dynamics (Vernet et al., 2008) and iron availability (Klunder et al., 2014). High concentrations of chlorophyll *a* and diatoms are distributed north of the Peninsula Front and at the SSI, while lower production and communities of nanoplanktonic flagellates are found between the Peninsula Front and the WAP (Gonçalves-Araujo et al., 2015). Further, changes in coastal primary production are driven by upwelling, iron distribution and the retreat of sea ice cover in spring releasing nutrients and stabilizing the water column (Vernet et al., 2008). A close link between marine primary production at the surface and sediment composition at the ocean floor is reflected in high concentrations of total organic carbon (TOC), pigments, sterols and diatoms (Cárdenas et al., 2019), and supported by studies confirming high fluxes of sinking particles (Kim et al., 2004; Wefer et al., 1988). In the study area, particle flux is highly variable with seasonal peaks occurring in late spring, which accounts for 85% of the total flux (Ducklow et al., 2008). Lithologically, the sediments consist mainly of terrestrial silt and clay with varying amounts of diatom mud and ooze, and sand (Cádiz Hernández, 2019; Lamy, 2016; Wu et al., 2019).

2.2 Sediment samples and age model

Piston core PS97/072-1 (62° 0.39’ S, 56° 3.86’ W, 1993 m water depth, 1583 cm in length) was recovered in the eastern Bransfield Strait Basin during R/V *Polarstern* cruise PS97 (Lamy, 2016) (Fig. 1). The core is dominated

https://doi.org/10.5194/egusphere-2022-804
Preprint. Discussion started: 24 August 2022

by silt with thin layers of sand, clay, and traces of volcanic ash. Single pebbles are present below 630 cm. Since we found disturbed sediments below 1015 cm depth, we only considered samples from above this level for our analyses. After an XRF scan the core sampling was done at the Alfred Wegener Institute (AWI) where the samples were stored frozen in glass vials (for biomarker analysis) and at 4° C in plastic bags (for micropaleontology).

The age model of core PS97/072-1 is based on ^{14}C radiocarbon dating of eight calcite samples with the mini carbon dating system (MICADAS) at AWI (Mollenhauer et al., 2021). From the conventional ^{14}C age we subtracted a reservoir age based on modelling by Butzin et al. (2017) and also subtracted an estimated ventilation age of 1200 years (see table supplement section 1) before we calibrated the ages with the calibration curve SHCal20 (Hogg et al., 2020) to calendar years before present (cal BP) with Calib 7.1 (Stuiver et al., 2018). To estimate the top age of the core, TOC and biogenic opal data of the piston core were matched with data from a multicore from the same sampling site that has been previously dated via ^{210}Pb (Vorrath et al., 2020) (supplement section 2). We applied the Bayesian age modelling tool *hummingage*, a freely available tool developed at AWI, that has been successfully applied in previous studies (Ronge et al., 2021).

2.3 Organic geochemical analyses of piston core PS97/072-1

For the analyses of several organic components and biomarkers the sediments were freeze-dried and homogenized in an agate mortar. Total carbon (C) and nitrogen (N) were measured with a CNS analyzer (Elementar Vario EL III, error of standards and duplicates < 5%). TOC was measured on 0.1 g of acidified samples (500 µl HCl) and determined in a carbon-sulphur determinator (CS-800, ELTRA, standard error < 0.6%). To identify the source of TOC, measurements of stable carbon isotopes of bulk organic matter were done at Universität Hamburg (UHH), Germany, and at Washington State University (WSU), USA. At UHH, the samples were acidified three times with 100 µl 1 N HCl and dried on a hotplate. High-temperature combustion was done in an Elementar CHNOS Vario isotope elemental analyser at 950° C and the analysis was conducted with an Elementar IsoPrime 100 isotope ratio mass spectrometer. We calibrated the pure tank CO_2 with the International Atomic Energy Agency reference standards IAEA-CH6 and IAEA-CH7. These and two other standards (IVA Sediment and Sucrose) acted as internal standards in the measurement. The error of continuous standard duplicates was < 0.2‰ and <0.06‰ for sample duplicates. At WSU, 100 mg of freeze-dried sediment samples were used. An elemental analyzer coupled with an Isoprime isotope ratio mass spectrometer (IRMS) was used, with a precision of 0.1‰. The running standard was a protein hydrolysate calibrated against NIST standards. Isotope ratios are expressed in units per mil (‰). $\delta^{13}C$ values are expressed in ‰ against Vienna Pee Dee Belemnite (VPDB).

Biogenic opal was estimated following the alkaline extraction procedure described by Mortlock and Froelich (1989), but using 0.5M NaOH as a digestion solution (Müller and Schneider, 1993). Extraction and analysis by

https://doi.org/10.5194/egusphere-2022-804
Preprint. Discussion started: 24 August 2022

molybdate-blue spectrophotometry were conducted at the University of Concepción, Chile. Values are expressed as biogenic opal by multiplying the Si (%) by 2.4 (Mortlock and Froelich, 1989). We did not correct for the release of extractable Si from coexisting clay minerals, and thus biogenic opal values could be slightly overestimated (Schlüter and Rickert, 1998). Instrumental precision was ±0.5%; error of duplicates ≤ 3%). Details on the methodology used can be found in Cárdenas et al. (2019).

The extraction, purification and identification of HBIs followed the analytical protocol published e.g. in Belt et al. (Belt et al., 2014) and Vorrath et al. (2019). 7-hexylnonadecane (7-HND) and C_{46} served as internal standards. Lipids were extracted using ultra sonication and a mixture of CH_2Cl_2:MeOH (v/v 2:1; 6ml). HBIs and GDGTs were separated by means of open column chromatography using SiO_2 as the stationary phase and hexane, and CH_2Cl_2:MeOH (v/v 1:1) as eluents. HBIs were analyzed by means of an Agilent 7890B gas chromatograph (30 m DB 1MS column, 0.25 mm diameter, 0.250 µm film thickness) coupled to an Agilent 5977B mass spectrometer (MSD, 70 eV constant ionization potential, ion source temperature 230° C). The initial oven temperature of 60° C was held for 3 min, ramped to 325° C within 23 min, and was held at 325° C for 16 min. HBIs were identified *via* comparison of their retention times and mass spectra with published mass spectra (Belt et al., 2000) and quantified using the ratio of peak areas of individual HBIs (*m/z* 346; *m/z* 348) and the 7-HND (*m/z* 266) standard and consideration of instrumental response factors. The error of duplicates was <1.4% for $IPSO_{25}$, <2.6% for HBI trienes. The phytoplankton-$IPSO_{25}$ index ($PIPSO_{25}$) was calculated after Vorrath et al. (2019) as:

$$PIPSO_{25} = \frac{IPSO_{25}}{IPSO_{25} + (c \times phytoplankton\ marker)} \ . \quad (1)$$

The HBI z-triene was considered as a phytoplankton biomarker and, since the concentrations were on the same level as $IPSO_{25}$, the c-factor was set to 1 (Vorrath et al., 2019). To confirm the sea-ice origin of $IPSO_{25}$, the stable carbon isotope composition of $IPSO_{25}$ was examined in 8 samples (with minimum 50 ng carbon) via GC-irm-MS at the GFZ Potsdam, Germany. The GC (7890N Agilent) equipped with Ultra1 column (50 m x 0.2 mm diameter, 0.33 µm film thickness) was connected to a DeltaVPlus isotope ratio mass spectrometer through a modified GC-Isolink interface. Each sample was separated chromatographically with a temperature program that started with an oven temperature of 80° C, which was held for 3 min, ramped to 250° C with 3° C per min and then ramped to 320° C with 5° C per min and finally reached temperature of 325° C with a ramp of 1° C per min and held for 15 min. The organic substances of the GC effluent stream were oxidized to CO_2 in the combustion furnace held at 940° C on a CuO/Ni/Pt catalyst. Samples were measured in duplicate and the standard deviation was ≤0.5 ‰. The quality of the isotope measurements was checked regularly by measuring different *n*-alkane standards with known isotopic composition (provided by Campro Scientific, Germany and Arndt Schimmelmann, Indiana University, USA).

GDGTs were re-dissolved in 120 µl hexane:isopropanol (v/v 99:1) and filtered through polytetrafluoroethylene filters (0.45 µm in diameter) and analyzed using high performance liquid chromatography (HPLC, Agilent 1200 series HPLC system) coupled to a single quadrupole mass spectrometer (MS, Agilent 6120 MSD) *via* an atmospheric pressure chemical ionization (APCI) interface. The individual GDGTs were separated at 30° C on a Prevail Cyano column (150 mm x 2.1 mm, 3µm). After injection of the sample (20 µl) it passed a 5 min isocratic elution with mobile phase A (hexane/2-propanol/chloroform; 98:1:1, flow rate 0.2 ml/min). The mobile phase B (hexane/2-propanol/chloroform; 89:10:1) was increased to 100% in two steps: a linear increase to 10% over 20 min followed by an increase to 100% within 10 min. During the measurement, the column was cleaned after 7 min *via* backflush (5 min, flow 0.6 ml/min) and re-equilibrated with solvent A (10 min, flow 0.2 ml/min). The conditions of the APCI were a nebulizer pressure of 50 psi, vaporizer temperature and N_2 drying gas temperature 350°C, flow 5 l/min, capillary voltage 4 kV, and corona current 5 µA. The GDGTs were detected by selective ion monitoring (SIM) of $(M+H^+)$ ions (dwell time 76 ms). In relation to the internal standard C_{46} (*m/z* 744) the molecular ions *m/z* of GDGTs-I (*m/z* 1300), GDGTs-II (*m/z* 1298), GDGTs-III (*m/z* 1296), and crenarchaeol (*m/z* 1292) were quantified. Also, the branched GDGTs-Ia (*m/z* 1022), GDGTs-IIa (*m/z* 1036), GDGTs-IIIa (*m/z* 1050) were quantified. The hydroxylated GDGTs OH-GDGT-0 (*m/z* 1318), OH-GDGT-1 (*m/z* 1316), and OH-GDGT-2 (*m/z* 1314) were quantified in the scans of their related GDGTs (Fietz et al., 2013). The standard deviation was 0.01 units of TEX^L_{86}.

Kalanetra et al. (2009) showed that GDGT-producing Thaumarchaeota are abundant in subsurface waters in both Arctic and Antarctic regions. As Thaumarchaeota were found between 50 m and 200 m water depth in Antarctica (Kim et al., 2012), temperatures based on GDGTs are suggested to reflect sub-surface waters (Etourneau et al., 2013, 2019). Similarly, also RI-OH' based temperatures in Prydz Bay have been interpreted to reflect subsurface water temperatures (Liu et al., 2020). We therefore consider our results to reflect subsurface ocean temperatures (SOTs). We calculated TEX^L_{86} after Kim et al. (2012) with the *m/z* 12963 (GDGT-3), *m/z* 1298 (GDGT-2), *m/z* 1300 (GDGT-1):

$$TEX^L_{86} = \log\left(\frac{[GDGT-2]}{[GDGT-1]+[GDGT-2]+[GDGT-3]}\right) \quad (2)$$

and calibrated with SOT = 50.8 * TEX^L_{86} + 36.1 (Kim et al., 2012). (3)

For the calculation of temperatures based on hydroxylated GDGTs we followed the approach of Lü et al. (2015)

$$RI-OH' = \frac{[OH-GDGT-1]+2\times[OH-GDGT-2]}{[OH-GDGT-0]+[OH-GDGT-1]+[OH-GDGT-2]} \quad (4)$$

and calibrated it with SOT = (RI-OH' - 0.1) / 0.0382. (5)

https://doi.org/10.5194/egusphere-2022-804
Preprint. Discussion started: 24 August 2022

For the branched and isoprenoid tetraether (BIT) index for indicating terrestrial organic matter (Hopmans et al., 2004) we used crenarchaeol (m/z 1292) and the branched GDGTs and calculated it as:

$$BIT = \frac{[GDGT-Ia]+[GDGT-IIa]+[GDGT-IIIa]}{[Crenarchaeol]+[GDGT-Ia]+[GDGT-IIa]+[GDGT-IIIa]}. \quad (6)$$

2.4 Diatom analyses

We selected a set of 76 samples for the analysis of diatom assemblages. Freeze-dried samples (20-120 mg) were treated with hydrogen peroxide and sodium pyrophosphate to remove organic matter and clays, respectively, washed several times with DI water until reaching neutral pH. The treated samples were then settled for six hours in B-Ker2 settling chambers to promote an even distribution of settled particles (Scherer, 1994; Schrader and Gersonde, 1978; Warnock and Scherer, 2014). Once the samples were dry, the quantitative slides were mounted with Norland mounting medium (refraction index=1.56). Diatom valves per slide were counted across traverses (at least 400 valves per slide) using an Axioscop 2 Plus and Olympus BX60 at a magnification of ×1000. The counting procedure and definition of counting units followed those of Schrader and Gersonde (1978). We performed two sets of counts, with and without *Chaetoceros* resting spores. Diatoms were identified to species or species group level and, if applicable, to variety or form level following the taxonomy described by e.g., Gersonde and Zielinski (2000), Armand and Zielinski (2001), Esper et al. (2010), Esper and Gersonde (2014a, 2014b). Diatom studies were done at the University of Concepción, Chile, and at Colgate University, USA.

Diatom species were grouped into ecological assemblages reflecting i) seasonal sea-ice, ii) cold open ocean, iii) warmer open ocean, and iv) benthic-epiphytic diatoms environments (Buffen et al., 2007; Cárdenas et al., 2019; Esper et al., 2010). Additionally, a group of reworked diatoms was identified. A Spearman principal component analysis (PCA) was applied to the diatom assemblages to differentiate their temporal distribution.

For estimation of winter sea ice (WSI) concentrations we applied the transfer function MAT-D274/28/4an which comprises 274 reference samples with 28 diatom taxa/taxa groups and considers an average of 4 analogues (Esper and Gersonde, 2014a). The analogues refer to surface sediments from the Atlantic, Pacific and western Indian sector of the Southern Ocean. The WSI renders sea-ice concentrations in a 1° by 1° grid for the September average of the period 1981 to 2010 (Reynolds et al., 2002, 2007). The threshold of an open ocean to sea ice covered area is set at 15% of sea ice concentration (Zwally et al., 2002) and the average sea ice edge is defined at 40% (Gersonde et al., 2005; Gloersen et al., 1993). The qualitative estimation of sea ice concentration was derived from the abundance pattern of diatom sea-ice indicators (Gersonde and Zielinski, 2000). The estimation of summer sea surface temperature (SSST) came from the transfer function IKM-D336/29/3q comprising 336 reference samples (Pacific, Atlantic and Indian Southern Ocean) with 29 diatom taxa and three factors (Esper and Gersonde, 2014b).

https://doi.org/10.5194/egusphere-2022-804
Preprint. Discussion started: 24 August 2022

The calculations were done with the software R (R Core Team, 2012) using the packages Vegan (Oksanen et al., 2012) and Analogue (Simpson and Oksanen, 2012).

3 Results

Based on our age model the sediment core covers the last 13.9 ka BP with a mean sedimentation rate of 67 cm/ka and a resolution ranging between 50 and 150 years per sample. We note a higher sedimentation rate of 95 cm/ka between 5.5 ka and 3 ka BP and few short-term intervals of significantly lowered (19 cm/ka) and enhanced (190 cm/ka) sedimentation (Fig. 2).

Organic geochemical bulk parameters (TOC, biogenic opal), concentrations of HBIs ($IPSO_{25}$, $C_{25:3}$ HBI triene) and diatom species assemblages of piston core PS97/072-1 are summarized in Figure 3 (additional data can be found in the supplement section 3). TOC increases from very low values of 0.1 wt% at 13.7 ka BP to an average concentration of ~0.8 wt% between 9.9 ka BP and the top of the core with recurring short-lived minima during the Middle and Late Holocene (Fig. 3f). Some of these TOC minima may be associated with thin sandy layers of volcanic ash. Biogenic opal shows a similar pattern with minimum values in the lower part of the record (3.2 wt% at 13.0 ka BP) and increases throughout the Deglacial to Holocene with average values of 30 wt% and a maximum of 54.4 wt% at 5.3 ka BP (Fig. 3e).

Between 13.9 ka and 13.4 ka BP, both $IPSO_{25}$ and HBI triene concentrations are close to or below the detection limit. The $IPSO_{25}$ concentration ranges between 0.1 to 31.5 µg g^{-1} TOC, while the concentration of the HBI triene ranges between 0.1 and 6.6 µg g^{-1} TOC (Fig. 3). $IPSO_{25}$ is absent before 13.5 ka BP and rises rapidly to maximum values at 12.9 ka BP. Subsequently, concentrations decrease steadily until 8.5 ka BP and then remain on an average level of ~4 µg g^{-1} TOC with a slightly decreasing trend towards the present and smaller peaks at 6.0 and 3.0 ka BP. The HBI triene is largely absent until 13.0 ka BP and shows high concentrations after 8.5 ka BP with large fluctuations in the Middle Holocene and from 3.4 ka BP to the present.

The diatom composition has two contrasting groups indicating open ocean conditions (Fig. 3a) and seasonal sea ice (Fig. 3c). Although the group reflecting seasonal sea ice is also present throughout the core (mostly >20%), the highest contributions are seen before 12.8 ka BP, between 10.8 and 9.9 ka BP and around 3 ka BP. The contribution of the open ocean assemblage is very low in the Deglacial and Early Holocene and rises to highest values in the Middle Holocene and remains around 10% in the Late Holocene. A biplot of a principal component analysis (PCA) shows the relationship of the ecological groups along the sediment core with clear dominance of seasonal sea-ice before 13.3 ka BP and warmer open ocean conditions after 8.5 ka BP (supplement section 4).

Sea ice estimates based on diatom assemblages (WSI) and the $PIPSO_{25}$ index as well as the content of IRD in PS97/72-1 are summarized in figure 4 (a-c). Reconstructed winter sea ice concentrations (% WSI) derived from diatom assemblages range from 80% to 90% during the ACR and the Deglacial (13.9 ka – 11 ka BP) and exhibit an overall decreasing trend over the Holocene with distinct fluctuations reaching minimum sea ice concentrations of ca. 65% during the Middle and Late Holocene (Fig. 4a). $PIPSO_{25}$ values show a similar trend indicating higher sea ice cover during the ACR, the Deglacial and the Early Holocene ($PIPSO_{25}$ > 0.8) and a successive decline throughout the Middle and Late Holocene with a distinct minimum at 0.5 ka BP (Fig. 4b). IRD (lithic particles and pebbles > 5 µm) occurs frequently between 13.9 ka and 9 ka BP and is virtually absent in the younger part of the sediment core (Fig. 4c).

Figure 5 provides ocean temperature reconstructions based on diatom assemblages (SSST) and GDGT-derived RI-OH' and TEX_{86}^{L} SOTs in core PS97/72-1 (Fig. 5 b-d). SSST estimates derived from diatom data generally have minimum temperatures of -1.5°C to 0°C during the Deglacial and a warming trend (> 0°C) in the Middle and Late Holocene with a distinct cold event at 3.1 ka BP (Fig. 5b). RI-OH'-derived SOTs reflect generally lower temperatures between -1.9 to -1.2°C and a similar trend of rising temperatures until 4.2 ka BP followed by a subtle cooling (Fig. 5c). TEX_{86}^{L} data from GDGTs cover a temperature range of 0.7 to 3.8°C and display an opposite trend to both SSST and RI-OH' SOT with decreasing temperatures since the Deglacial (Fig. 5d).

4 Discussion

4.1 The late Deglacial (14 ka to 11.7 ka BP)

In the oldest part of our sediment record covering the later part of the last Deglacial from 14 ka until 11.7 ka BP we observe a remarkable environmental change indicated by significant shifts in the TOC, biomarker and diatom records. Before 13.4 ka BP, the very low concentrations of biomarkers, TOC, and biogenic opal suggest that primary production associated with open marine and also sea ice settings was diminished, while sea-ice related diatom species show the highest contribution (Fig. 3) albeit very low concentrations (supplement section 5). Highest $PIPSO_{25}$ and WSI values pointing towards maximum sea ice cover and lowest ocean temperatures reflected in the RI-OH'-derived SOTs are well in line with peak ssNa concentrations and minimum $\delta^{18}O$ values in the EDML, WAIS and JRI ice core records referring to an extended sea ice cover and lowered atmospheric temperatures (Fig. 4 and 5; EPICA Community Members, 2006; Fischer et al., 2007; Mulvaney et al., 2012; WAIS Divide Project Members, 2015; WAIS Divide Project Members et al., 2013). The near absence of $IPSO_{25}$, HBI triene and open ocean diatom species between 13.9 ka and 13.5 ka BP evidences a very thick or permanent sea ice cover. Similarly, Lamping et al. (2020) relate the absence of $IPSO_{25}$ and a phytoplankton biomarker in sediments in the western Amundsen Sea to the re-advance of a floating ice shelf canopy during the ACR. The abrupt increase

https://doi.org/10.5194/egusphere-2022-804
Preprint. Discussion started: 24 August 2022

in $IPSO_{25}$ concentrations at 13.5 ka BP, may indicate the retreat of such an ice-shelf cover from the core site permitting sea ice growth during spring and a subsequent increase in primary production reflected in rapidly rising HBI triene concentrations at 13 ka BP. A significant decrease in sea ice associated diatoms between 13 ka and 12 ka BP (Fig. 3), however, is not mirrored by the still high WSI. We note that traces of biomarkers and diatoms (supplement section 5) deposited in sediments older than 13.5 ka BP may reflect sub-ice shelf lateral advection and reworking (Smith et al., 2019).

While the ACR lasts from 14.7 ka to 13 ka BP (Pedro et al., 2016), our sediment record shows that cold conditions with extended sea ice cover and reduced ocean temperatures in the eastern Bransfield Strait lasted until ca. 11 ka BP (Figs. 4 and 5). Further, the IRD content (including the presence of single large pebbles) points to the frequent occurrence of icebergs during the Deglacial and the Early Holocene (Fig. 4c) related to the overall ice sheet disintegration at the WAP that occurred around 14 ka BP at the South Shetland Islands and at 13.2 ka BP at Palmer Deep at the southern WAP (Domack et al., 2001; Domack, 2002; Jones et al., 2022; Milliken et al., 2009). A slight decrease in $PIPSO_{25}$ values and rising RI-OH' SOTs characterize the late Deglacial between 13 ka and 11.7 ka BP. This warming may relate to inter-hemispheric teleconnections through a global reorganization of atmospheric and ocean circulation that is related to the bipolar seesaw pattern of opposite climate trends between the northern and southern hemisphere (Anderson et al., 2009; Broecker, 1998; EPICA Community Members, 2006; Pedro et al., 2016). With cooling of the northern hemisphere, a southward shift of the Intertropical Convergence Zone and the southern hemisphere westerlies (Lamy et al., 2007) resulted in intensified wind stress in the Drake Passage (Timmermann et al., 2007) and increased upwelling that may have driven the continued warming and sea ice retreat in Antarctica towards the Holocene (Anderson et al., 2009).

4.2 Early Holocene warming from 11.7 ka to 8.2 ka BP

The Early Holocene from 11.7 ka to 8.2 ka BP is characterized by a progressively decreasing though highly variable winter and spring sea ice cover as shown by further declining WSI and $PIPSO_{25}$ values (Fig. 4a and b). While biogenic opal and TOC contents exhibit increasing trends, concentrations of the HBI triene and open ocean diatoms remain low and only a significant increase after 9 ka BP suggests higher phytoplankton productivity (Fig. 3). Ocean warming is indicated by RI-OH'-based SOT, while TEX_{86}^{L} SOT and diatom-derived SSST show fluctuating temperatures without a clear trend (Fig. 5b, c and d).

While $PIPSO_{25}$ values display a rather gradual decrease in sea ice coverage, the WSI record suggests a highly variable sea ice cover with few distinct sea ice minima between 11 ka and 10 ka BP and around 9 ka BP (Fig. 4a and b). These sea ice minima may have resulted from punctuated warming events, e.g. at 10 ka BP, when SSST shows a short temperature peak, which might have led to a delayed sea ice formation in autumn and winter (Fig.

https://doi.org/10.5194/egusphere-2022-804
Preprint. Discussion started: 24 August 2022

5b). Another WSI minimum at 9 ka BP coincides with a major (and final) peak in IRD deposition at the core site (Fig. 4) evidencing iceberg discharge during episodes of peak ice-sheet loss at the WAP (Jones et al., 2022). As sea ice melting may have been an important driver of the ocean stratification, we suggest warmer, stratified surface waters with moderate production in summer, supported by increasing insolation in December (Fig. 5a). Ameliorating climate conditions, ice-shelf retreat and the establishment of modern-like ocean conditions after 9 ka BP have also been proposed for the western Bransfield Strait (Heroy et al., 2008) and are well in line with the rising contribution of open ocean diatoms and the phytoplankton-derived HBI triene at our core site (Fig. 3). Our marine records of decreasing sea ice and rising ocean temperatures are consistent with the overall slight warming trend recorded in the WAIS Divide ice core (Fig. 5h). Interestingly, neither this rise in RI-OH' derived SOTs nor the highly variable TEX_{86}^{L} temperatures correspond to the declining TEX_{86} temperatures reported for ODP site 1098 at Palmer Deep (Shevenell et al., 2011) or the declining δD values recorded in the JRI ice core (Fig. 5; Mulvaney et al., 2012). These regional differences may relate to changing ocean circulation patterns and associated shifts in water mass distribution at the WAP and EAP during the Early Holocene. We further note that the partly opposing trends in RI-OH' and TEX_{86}^{L} temperatures at our core site could indicate that the respective GDGT producing archaea thrive in different water depths or during different seasons.

4.3 Middle Holocene from 8.2 ka until 4.2 ka BP

The Middle Holocene from 8.2 ka to 4.2 ka BP is a period of significant sea ice retreat and minimum iceberg flux at the core site indicated by decreasing WSI and $PIPSO_{25}$ values, virtually absent IRD, and an oceanic warming reflected in SSST and RI-OH' SOT (Fig. 4 and 5). For the whole period, diatoms associated with warmer open ocean conditions, peak HBI triene concentrations and maximum TOC and biogenic opal contents (Fig. 3) refer to a high export production during the Middle Holocene (Abelmann et al., 2006; Smetacek et al., 2004). This can be linked to a decrease of both winter and spring sea ice and potentially ice-free summers indicated by WSI and $PIPSO_{25}$ minima (Fig. 4).

The retreat of the previously grounded AP ice-sheet between 10 ka and 5 ka BP finally opened the passage for ACC surface waters to enter the Bransfield Strait from the west (Bentley et al., 2014; Ó Cofaigh et al., 2014). As a result, we suggest that sea ice conditions at our core site were predominantly influenced by branches of the ACC (the BSW and CDW) and inflow from the Weddell Sea was diminished due to the still grounded ice sheet at the tip of the AP. The influence from the Weddell Sea was weak and opposite sea ice conditions were reconstructed for the eastern AP where HBI biomarker and diatom assemblages record extended sea ice cover between 7 ka and 4.5 ka BP (Fig. 4e, Barbara et al., 2016a; Minzoni et al., 2015).

https://doi.org/10.5194/egusphere-2022-804
Preprint. Discussion started: 24 August 2022

Regarding ocean temperatures, we observe a sustained warming in RI-OH' SOT punctuated by a cooling at 5.5 ka BP, while TEX_{86}^{L} temperatures depict a subtle cooling between 8.2 ka and 7 ka BP followed by a warm reversal until 6 ka BP (Fig. 5). A Middle Holocene slight cooling trend has also been observed at core sites at Palmer Deep at the WAP (Fig. 1 and 5, Etourneau et al., 2013; Shevenell et al., 2011) and contrasts a rapid warming observed in JPC38 from the eastern AP between 8 ka and 6.5 ka BP (Fig. 1 and 5, Barbara et al., 2016; Etourneau et al., 2019). Here, the near-coastal marine sediment core close to JRI (Fig. 5g, Barbara et al., 2016) records the transition from cold and heavily sea ice covered conditions at 8.2 ka BP to a warmer environment with reduced ice cover permitting phytoplankton growth between 6.5 ka and 4.2 ka BP (Barbara et al., 2016). Since stable temperatures are inferred from the JRI ice core during the entire Middle Holocene (Mulvaney et al., 2012), we suggest that the environmental changes recorded in JPC38 reflect ocean-driven rather than atmospheric processes.

4.4 Late Holocene and Neoglacial from 4.2 ka BP until today

The Late Holocene covering the past 4.2 ka BP is characterized by relatively stable environmental conditions at our core site reflected in constant biogenic opal and TOC contents, low $IPSO_{25}$ and still variable but elevated HBI triene concentrations. A gradual decline in $PIPSO_{25}$ values between 4.2 ka and 1.5 ka BP contrasts the highly variable WSI concentrations (Fig. 4). Minimum $PIPSO_{25}$ values at 0.5 ka BP are related to the significantly reduced $IPSO_{25}$ and HBI triene concentrations. Similar to our observation for the Deglacial, this pattern of low HBI triene and minimum $IPSO_{25}$ concentrations may point to perennial cold conditions and the establishment of thick and/or compacted sea ice limiting the productivity of both phytoplankton and also sea ice diatoms. This short period of sea ice growth may be related to the Little Ice Age (LIA), when cooler conditions also triggered glacial readvance at the Antarctic Peninsula 500 years ago (*e.g.* Simms et al., 2021). While a significant pulse in sea ice export from the Arctic Ocean is proposed to have caused the LIA cooling (Miles et al., 2020), knowledge about LIA sea ice conditions in the Southern Ocean is scarce and hence inconclusive (Parkinson, 1990). The Neoglacial cooling as found in the JRI ice core, for example, is clearly reflected in an increased sea ice cover at Palmer Deep since 2 ka BP (Fig. 4d, Etourneau et al., 2013) but this record, however, contains no clear evidence for a further expansion of sea ice in response to the LIA. We conclude that a comprehensive assessment of how Antarctic sea ice conditions changed during the LIA requires more studies of well-dated and ideally higher resolved sediment records.

Similar to our sea ice signals, also the Late Holocene ocean temperature reconstructions display different patterns. While RI-OH' SOT remains relatively stable, TEX_{86}^{L} indicates a cooling around 3 ka BP followed by a warming until 1.5 ka BP and another cooling towards the top of the core. Diatom-derived SSST also point to a cold period

https://doi.org/10.5194/egusphere-2022-804
Preprint. Discussion started: 24 August 2022

around 3 ka BP immediately followed by a warming peak at ca. 2.5 ka BP. Evidently, temperature trends at the WAP in the Late Holocene are highly variable between different areas (Allen et al., 2010; Barbara et al., 2016; Bárcena et al., 1998; Bentley et al., 2009; Etourneau et al., 2013; Mulvaney et al., 2012; Shevenell et al., 2011) and this may relate to the complex oceanographic and atmospheric settings. With regard to the diverging temperature trends observed in sediment core PS97/72-1, we not that also inconsistencies between different analytical approaches to reconstruct ocean temperatures need to be acknowledged and examined. As previously stated, more information on the applicability and significance of GDGT-derived ocean temperatures in polar latitudes is needed.

5 Conclusions

We reconstructed the sea ice and climate development at the northwest AP since the last Deglacial using the sediment core PS97/072-1 from the Bransfield Strait. In our multiproxy study we focused on the sea ice biomarker $IPSO_{25}$, the HBI z-triene representing open marine environments, and GDGTs for ocean temperature reconstructions. Diatom ecological groups characteristic of sea ice or open ocean conditions were used, as well as diatom transfer functions to reconstruct winter sea ice and summer sea surface temperature. Additional information was derived from sedimentological records such as IRD. Our results reveal the retreat of a floating ice shelf canopy after the ACR and an overall sea ice retreat and ocean warming during the Holocene. The late Deglacial from 13.9 ka to 11.7 ka BP was a highly dynamic period: until 13.4 ka BP the sedimentation of organic proxies was diminished due to a permanent ice cover during the ACR. The ACR terminated with a shift to warm conditions at 13 ka BP along with a retreat in spring sea ice. The Early Holocene from 11.7 ka to 8.2 ka BP was characterized by warming, slightly decreasing spring sea ice cover and highly variable winter sea ice cover. In the Middle Holocene from 8.2 ka to 4.2 ka BP, stable environmental conditions prevailed with elevated primary production due to intervals of lower sea ice cover. In general, sea ice seasons were short and sea ice cover was significantly reduced to a minimum around 5.5 ka BP, even though high seasonal amplitudes and short-term, centennial changes in sea ice conditions occurred. During the Late Holocene, the core site experienced a variable WSI and a short-term cooling at 3 ka BP. Phytoplankton biomarkers as well as sea ice proxies ($IPSO_{25}$, $PIPSO_{25}$, WSI) were lowest during the period coincident with the Little Ice Age which we relate to the establishment of a multi-year sea ice cover.

Data Availability

All data mentioned in this paper will be available at the open access repository www.pangaea.de (https://doi.pangaea.de/10.1594/XXXXXXX).

Author contributions

The study was conceived by MV and JM. Data collections and experimental investigations were done by MV together with LLJ (foraminifera, age model), SMS (age model, humming age), CBL (core description, sampling, diatoms, biogenic opal, age model), PC (diatoms), AL (age model, diatoms), OE (diatom transfer function), GM (GDGTs PS97/072-1, ^{14}C dating), AVH ($\delta^{13}C$ $IPSO_{25}$), NL ($\delta^{13}C$ TOC), Je, DE and CE provided temperature and salinity profiles near the study site. MV drafted the manuscript. All authors contributed to the interpretation and discussion of the data and the finalization of this manuscript.

Competing interests

None of the authors have a conflict of interest.

Acknowledgement

We thank the captain, crew and chief scientist Frank Lamy of RV Polarstern cruise PS97. Denise Diekstall, Jens Hefter, Alejandro Avila and Victor Acuña are thanked for their laboratory support. We thank Helge Arz for his help with the age model. Simon Belt is acknowledged for providing the 7-HND internal standard for HBI quantification. Financial support was provided through the Helmholtz Research grant VH-NG-1101. Partial support from the Centers IDEAL (grant FONDAP 15150003) and COPAS Sur-Austral (AFB170006), Chile, and the Spanish Ministry of Economy, Industry and Competitivity grants CTM2017-89711-C2-½-P, co-funded by the European Union through FEDER funds, is acknowledged. We acknowledge support by the Open Access Publication Funds of Alfred-Wegener-Institut Helmholtz-Zentrum für Polar- und Meeresforschung.

References

Abelmann, A., Gersonde, R., Cortese, G., Kuhn, G. and Smetacek, V.: Extensive phytoplankton blooms in the Atlantic sector of the glacial Southern Ocean, Paleoceanography, 21(1), 1–9, doi:10.1029/2005PA001199, 2006.

Alexander, V. and Niebauer, H. .: Oceanography of the eastern Bering Sea ice-edge zone in spring, Limn, 26(6), 1111–1125 [online] Available from: http://doi.wiley.com/10.1029/2007RG000250, 1981.

Allen, C. S., Oakes-Fretwell, L., Anderson, J. B. and Hodgson, D. A.: A record of Holocene glacial and oceanographic variability in Neny Fjord, Antarctic Peninsula, The Holocene, 20(4), 551–564, doi:10.1177/0959683609356581, 2010.

Allison, I., Tivendale, C. M., Akerman, G. J., Tann, J. M. and Wills, R. H.: Seasonal Variations In The Surface Energy Exchanges Over Antarctic Sea Ice and Coastal Waters, Annals of Glaciology, 3, 12–16, doi:10.3189/S0260305500002445, 1982.

Anderson, R. F., Ali, S., Bradtmiller, L. I., Nielsen, S. H. H., Fleisher, M. Q., Anderson, B. E. and Burckle, L. H.: Wind-Driven Upwelling in the Southern Ocean and the Deglacial Rise in Atmospheric CO2, Science, 323, 1443–1448, doi:10.1126/science.1167441, 2009.

Armand, L. K. and Zielinski, U.: DIATOM SPECIES OF THE GENUS *RHIZOSOLENIA* FROM SOUTHERN OCEAN SEDIMENTS: DISTRIBUTION AND TAXONOMIC NOTES, Diatom Research, 16(2), 259–294, doi:10.1080/0269249X.2001.9705520, 2001.

Arrigo, K. R., Worthen, D. L., Lizotte, M. P., Dixon, P. and Dieckmann, G.: Primary Production in Antarctic Sea Ice, Science, 276, 394–397, doi:10.1126/science.276.5311.394, 1997.

Barbara, L., Crosta, X., Schmidt, S. and Massé, G.: Diatoms and biomarkers evidence for major changes in sea ice conditions prior the instrumental period in Antarctic Peninsula, Quaternary Science Reviews, 79, 99–110, doi:10.1016/j.quascirev.2013.07.021, 2013.

Barbara, L., Crosta, X., Leventer, A., Schmidt, S., Etourneau, J., Domack, E. and Massé, G.: Environmental responses of the Northeast Antarctic Peninsula to the Holocene climate variability, Paleoceanography, 31(1), 131–147, doi:10.1002/2015PA002785, 2016.

Bárcena, M. A., Gersonde, R., Ledesma, S., Fabrés, J., Calafat, A. M., Canals, M., Sierro, F. J. and Flores, J. A.: Record of Holocene glacial oscillations in Bransfield Basin as revealed by siliceous microfossil assemblages, Antarctic Science, 10(03), 269–285, doi:10.1017/S0954102098000364, 1998.

Belt, S. T., Allard, W. G., Massé, G., Robert, J. M. and Rowland, S. J.: Highly branched isoprenoids (HBIs): Identification of the most common and abundant sedimentary isomers, Geochimica et Cosmochimica Acta, 64(22), 3839–3851, doi:10.1016/S0016-7037(00)00464-6, 2000.

https://doi.org/10.5194/egusphere-2022-804
Preprint. Discussion started: 24 August 2022

Belt, S. T., Brown, T. A., Ampel, L., Cabedo-Sanz, P., Fahl, K., Kocis, J. J., Massé, G., Navarro-Rodriguez, A., Ruan, J. and Xu, Y.: An inter-laboratory investigation of the Arctic sea ice biomarker proxy IP₂₅ in marine sediments: key outcomes and recommendations, Climate of the Past, 10(1), 155–166, doi:10.5194/cp-10-155-2014, 2014.

Belt, S. T., Smik, L., Brown, T. A., Kim, J. H., Rowland, S. J., Allen, C. S., Gal, J. K., Shin, K. H., Lee, J. I. and Taylor, K. W. R.: Source identification and distribution reveals the potential of the geochemical Antarctic sea ice proxy IPSO25, Nature Communications, 7, 1–10, doi:10.1038/ncomms12655, 2016.

Bentley, M. J., Hodgson, D. A., Smith, J. A., Cofaigh, C. ., Domack, E. W., Larter, R. D., Roberts, S. J., Brachfeld, S., Leventer, A., Hjort, C., Hillenbrand, C.-D. and Evans, J.: Mechanisms of Holocene palaeoenvironmental change in the Antarctic Peninsula region, The Holocene, 19(1), 51–69, doi:10.1177/0959683608096603, 2009.

Bentley, M. J., Ó Cofaigh, C., Anderson, J. B., Conway, H., Davies, B., Graham, A. G. C., Hillenbrand, C.-D., Hodgson, D. A., Jamieson, S. S. R., Larter, R. D., Mackintosh, A., Smith, J. A., Verleyen, E., Ackert, R. P., Bart, P. J., Berg, S., Brunstein, D., Canals, M., Colhoun, E. A., Crosta, X., Dickens, W. A., Domack, E., Dowdeswell, J. A., Dunbar, R., Ehrmann, W., Evans, J., Favier, V., Fink, D., Fogwill, C. J., Glasser, N. F., Gohl, K., Golledge, N. R., Goodwin, I., Gore, D. B., Greenwood, S. L., Hall, B. L., Hall, K., Hedding, D. W., Hein, A. S., Hocking, E. P., Jakobsson, M., Johnson, J. S., Jomelli, V., Jones, R. S., Klages, J. P., Kristoffersen, Y., Kuhn, G., Leventer, A., Licht, K., Lilly, K., Lindow, J., Livingstone, S. J., Massé, G., McGlone, M. S., McKay, R. M., Melles, M., Miura, H., Mulvaney, R., Nel, W., Nitsche, F. O., O'Brien, P. E., Post, A. L., Roberts, S. J., Saunders, K. M., Selkirk, P. M., Simms, A. R., Spiegel, C., Stolldorf, T. D., Sugden, D. E., van der Putten, N., van Ommen, T., Verfaillie, D., Vyverman, W., Wagner, B., White, D. A., Witus, A. E. and Zwartz, D.: A community-based geological reconstruction of Antarctic Ice Sheet deglaciation since the Last Glacial Maximum, Quaternary Science Reviews, 100(August), 1–9, doi:10.1016/j.quascirev.2014.06.025, 2014.

Blunier, T. and Brook, E. J.: Timing of millennial-scale climate change in antarctica and greenland during the last glacial period, Science, 291(5501), 109–112, doi:10.1126/science.291.5501.109, 2001.

Bracegirdle, T. J., Stephenson, D. B., Turner, J. and Phillips, T.: The importance of sea ice area biases in 21st century multimodel projections of Antarctic temperature and precipitation, Geophysical Research Letters, 42(24), 10,832-10,839, doi:10.1002/2015GL067055, 2015.

Bracegirdle, T. J., Colleoni, F., Abram, N. J., Bertler, N. A. N., Dixon, D. A., England, M., Favier, V., Fogwill, C. J., Fyfe, J. C., Goodwin, I., Goosse, H., Hobbs, W., Jones, J. M., Keller, E. D., Khan, A. L., Phipps, S. J., Raphael, M. N., Russell, J., Sime, L., Thomas, E. R., van den Broeke, M. R. and Wainer, I.: Back to the Future:

https://doi.org/10.5194/egusphere-2022-804
Preprint. Discussion started: 24 August 2022

Using Long-Term Observational and Paleo-Proxy Reconstructions to Improve Model Projections of Antarctic Climate, Geosciences, 9(6), 255, doi:10.3390/geosciences9060255, 2019.

Broecker, W. S.: Paleocean circulation during the Last Deglaciation: A bipolar seesaw?, Paleoceanography, 13(2), 119–121, doi:10.1029/97PA03707, 1998.

Buffen, A., Leventer, A., Rubin, A. and Hutchins, T.: Diatom assemblages in surface sediments of the northwestern Weddell Sea, Antarctic Peninsula, Marine Micropaleontology, 62(1), 7–30, doi:10.1016/J.MARMICRO.2006.07.002, 2007.

Butterworth, B. J. and Miller, S. D.: Air-sea exchange of carbon dioxide in the Southern Ocean and Antarctic marginal ice zone, Geophysical Research Letters, 43(13), 7223–7230, doi:10.1002/2016GL069581, 2016.

Butzin, M., Köhler, P. and Lohmann, G.: Marine radiocarbon reservoir age simulations for the past 50,000 years, Geophysical Research Letters, 44(16), 8473–8480, doi:10.1002/2017GL074688, 2017.

Cádiz Hernández, A.: Evidencia de cambios en la productividad marina a partir de testigos sedimentarios recuperados en Bahía Fildes (Maxwell Bay) y Costa de Palmer, Península Antártica durante los últimos ~ 1000 años, Universidad de Valparaíso., 2019.

Canals, M. and Amblas, D.: Seafloor kettle holes in Orleans Trough, Bransfield Basin, Antarctic Peninsula, Geological Society, London, Memoirs, 46(1), 313–314, doi:10.1144/M46.16, 2016a.

Canals, M. and Amblas, D.: The bundle: a mega-scale glacial landform left by an ice stream, Western Bransfield Basin, Geological Society, London, Memoirs, 46(1), 177–178, doi:10.1144/M46.157, 2016b.

Canals, M., Amblas, D. and Casamor, J. L.: Cross-shelf troughs in Central Bransfield Basin, Antarctic Peninsula, Geological Society, London, Memoirs, 46(1), 171–172, doi:10.1144/M46.138, 2016.

Cárdenas, P., Lange, C. B., Vernet, M., Esper, O., Srain, B., Vorrath, M.-E. M.-E., Ehrhardt, S., Müller, J., Kuhn, G., Arz, H. W. H. W. H. W., Lembke-Jene, L., Lamy, F. and Paola Cárdenas, Carina B. Lange, Maria Vernet, Oliver Esper, Benjamin Srain, Maria-Elena Vorrath, Sophie Ehrhardt, Juliane Müller, Gerhard Kuhn, Helge W.Arz, Lester Lembke-Jene, F. L.: Biogeochemical proxies and diatoms in surface sediments across the Drake Passage reflect oceanic domains and frontal systems in the region, Progress in Oceanography, 174, 72–88, doi:10.1016/j.pocean.2018.10.004, 2019.

Chisholm, S. W.: Stirring times in the Southern Ocean, Nature, 407(6805), 685–686, doi:10.1038/35037696, 2000.

Clark, P. U., Shakun, J. D., Baker, P. A., Bartlein, P. J., Brewer, S., Brook, E., Carlson, A. E., Cheng, H., Kaufman, D. S., Liu, Z., Marchitto, T. M., Mix, A. C., Morrill, C., Otto-Bliesner, B. L., Pahnke, K., Russell, J. M., Whitlock, C., Adkins, J. F., Blois, J. L., Clark, J., Colman, S. M., Curry, W. B., Flower, B. P., He, F., Johnson, T. C., Lynch-Stieglitz, J., Markgraf, V., McManus, J., Mitrovica, J. X., Moreno, P. I. and Williams, J. W.: Global climate evolution during the last deglaciation, Proceedings of the National Academy of Sciences, 109(19), E1134–E1142, doi:10.1073/pnas.1116619109, 2012.

Collares, L. L., Mata, M. M., Kerr, R., Arigony-Neto, J. and Barbat, M. M.: Iceberg drift and ocean circulation in the northwestern Weddell Sea, Antarctica, Deep Sea Research Part II: Topical Studies in Oceanography, 149(January 2019), 10–24, doi:10.1016/j.dsr2.2018.02.014, 2018.

Cook, A. J., Holland, P. R., Meredith, M. P., Murray, T., Luckman, A. and Vaughan, D. G.: Ocean forcing of glacier retreat in the western Antarctic Peninsula, Science, 353(6296), 283–286, doi:10.1126/science.aae0017, 2016.

Crosta, X., Kohfeld, K. E., Bostock, H. C., Chadwick, M., Du Vivier, A., Esper, O., Etourneau, J., Jones, J., Leventer, A., Müller, J., Rhodes, R. H., Allen, C. S., Ghadi, P., Lamping, N., Lange, C. B., Lawler, K.-A., Lund, D., Marzocchi, A., Meissner, K. J., Menviel, L., Nair, A., Patterson, M., Pike, J., Prebble, J. G., Riesselman, C., Sadatzki, H., Sime, L. C., Shukla, S. K., Thöle, L., Vorrath, M.-E., Xiao, W. and Yang, J.: Antarctic sea ice over the past 130,000 years, Part 1: A review of what proxy records tell us, EGUsphere [preprint], doi:10.5194/egusphere-2022-99, 2022.

Denis, D., Crosta, X., Barbara, L., Massé, G., Renssen, H., Ther, O. and Giraudeau, J.: Sea ice and wind variability during the Holocene in East Antarctica: insight on middle–high latitude coupling, Quaternary Science Reviews, 29(27–28), 3709–3719, doi:10.1016/J.QUASCIREV.2010.08.007, 2010.

Domack, E., Leventer, A., Dunbar, R., Taylor, F., Brachfeld, S. and Sjunneskogs, C.: Chronology of the Palmer Deep site, Antarctic Peninsula: a Holocene palaeoenvironmental reference for the circum-Antarctic, The Holocene, 11(1), 1–9, doi:10.1191/095968301673881493, 2001.

Domack, E. W.: A Synthesis for Site 1098: Palmer Deep, in Proceedings of the Ocean Drilling Program, 178 Scientific Results, Ocean Drilling Program., 2002.

Ducklow, H. W., Erickson, M., Kelly, J., Montes-Hugo, M., Ribic, C. A., Smith, R. C., Stammerjohn, S. E. and Karl, D. M.: Particle export from the upper ocean over the continental shelf of the west Antarctic Peninsula: A long-term record, 1992–2007, Deep Sea Research Part II: Topical Studies in Oceanography, 55(18–19), 2118–2131, doi:10.1016/j.dsr2.2008.04.028, 2008.

EPICA Community Members: Eight glacial cycles from an Antarctic ice core, Nature, 429(6992), 623–628, doi:10.1038/nature02599, 2004.

EPICA Community Members: One-to-one coupling of glacial climate variability in Greenland and Antarctica, Nature, 444(7116), 195–198, doi:10.1038/nature05301, 2006.

Escutia, C., DeConto, R., Dunbar, R., De Santis, L., Shevenell, A. and Nash, T.: Keeping an Eye on Antarctic Ice Sheet Stability, Oceanography, 32(1), 32–46, doi:10.5670/oceanog.2019.117, 2019.

Esper, O. and Gersonde, R.: New tools for the reconstruction of Pleistocene Antarctic sea ice, Palaeogeography, Palaeoclimatology, Palaeoecology, 399, 260–283, doi:10.1016/J.PALAEO.2014.01.019, 2014a.

Esper, O. and Gersonde, R.: Quaternary surface water temperature estimations: New diatom transfer functions for the Southern Ocean, Palaeogeography, Palaeoclimatology, Palaeoecology, 414, 1–19, doi:10.1016/J.PALAEO.2014.08.008, 2014b.

Esper, O., Gersonde, R. and Kadagies, N.: Diatom distribution in southeastern Pacific surface sediments and their relationship to modern environmental variables, Palaeogeography, Palaeoclimatology, Palaeoecology, 287(1–4), 1–27, doi:10.1016/J.PALAEO.2009.12.006, 2010.

Etourneau, J., Collins, L. G., Willmott, V., Kim, J. H., Barbara, L., Leventer, A., Schouten, S., Sinninghe Damsté, J. S., Bianchini, A., Klein, V., Crosta, X. and Massé, G.: Holocene climate variations in the western Antarctic Peninsula: Evidence for sea ice extent predominantly controlled by changes in insolation and ENSO variability, Climate of the Past, 9(4), 1431–1446, doi:10.5194/cp-9-1431-2013, 2013.

Etourneau, J., Sgubin, G., Crosta, X., Swingedouw, D., Willmott, V., Barbara, L., Houssais, M. N., Schouten, S., Damsté, J. S. S., Goosse, H., Escutia, C., Crespin, J., Massé, G. and Kim, J. H.: Ocean temperature impact on ice shelf extent in the eastern Antarctic Peninsula, Nature Communications, 10(1), 8–15, doi:10.1038/s41467-018-08195-6, 2019.

Fietz, S., Huguet, C., Rueda, G., Hambach, B. and Rosell-Melé, A.: Hydroxylated isoprenoidal GDGTs in the Nordic Seas, Marine Chemistry, 152, 1–10, doi:10.1016/j.marchem.2013.02.007, 2013.

Fischer, H., Fundel, F., Ruth, U., Twarloh, B., Wegner, A., Udisti, R., Becagli, S., Castellano, E., Morganti, A., Severi, M., Wolff, E., Littot, G., Röthlisberger, R., Mulvaney, R., Hutterli, M. A., Kaufmann, P., Federer, U., Lambert, F., Bigler, M., Hansson, M., Jonsell, U., de Angelis, M., Boutron, C., Siggaard-Andersen, M.-L., Steffensen, J. P., Barbante, C., Gaspari, V., Gabrielli, P. and Wagenbach, D.: Reconstruction of millennial changes in dust emission, transport and regional sea ice coverage using the deep EPICA ice cores from the Atlantic and Indian Ocean sector of Antarctica, Earth and Planetary Science Letters, 260(1–2), 340–354, doi:10.1016/j.epsl.2007.06.014, 2007.

Gersonde, R. and Zielinski, U.: The reconstruction of late Quaternary Antarctic sea-ice distribution — the use of diatoms as a proxy for sea-ice, , 162, 263–286, doi:10.1016/S0031-0182(00)00131-0, 2000.

Gersonde, R., Crosta, X., Abelmann, A. and Armand, L.: Sea-surface temperature and sea ice distribution of the Southern Ocean at the EPILOG Last Glacial Maximum—a circum-Antarctic view based on siliceous microfossil records, Quaternary Science Reviews, 24(7–9), 869–896, doi:10.1016/J.QUASCIREV.2004.07.015, 2005.

Gloersen, P., Campbell, W. J., Cavalieri, D. J., Comiso, J. C., Parkinson, C. L. and Zwally, H. J.: Arctic and antarctic sea ice, 1978, Annals of Glaciology, 17, 149–154, 1993.

Gonçalves-Araujo, R., de Souza, M. S., Tavano, V. M. and Garcia, C. A. E.: Influence of oceanographic features on spatial and interannual variability of phytoplankton in the Bransfield Strait, Antarctica, Journal of Marine Systems, 142, 1–15, doi:10.1016/J.JMARSYS.2014.09.007, 2015.

Hellmer, H. H., Kauker, F., Timmermann, R., Determann, J. and Rae, J.: Twenty-first-century warming of a large Antarctic ice-shelf cavity by a redirected coastal current, Nature, 485(7397), 225–228, doi:10.1038/nature11064, 2012.

Heroy, D. C., Sjunneskog, C. and Anderson, J. B.: Holocene climate change in the Bransfield Basin, Antarctic Peninsula: evidence from sediment and diatom analysis, Antarctic Science, 20(01), 69–87, doi:10.1017/S0954102007000788, 2008.

Hillaire-Marcel, C. and de Vernal, A.: Proxies in Late Cenozoic Paleoceanography, edited by C. Hillaire-Marcel and A. de Vernal, Elsevier, Amsterdam., 2007.

Hofmann, E. E., Klinck, J. M., Lascara, C. M. and Smith, D. A.: Water mass distribution and circulation west of the Antarctic Peninsula and including Bransfield Strait, pp. 61–80, American Geophysical Union (AGU)., 1996.

Hogg, A. G., Heaton, T. J., Hua, Q., Palmer, J. G., Turney, C. S., Southon, J., Bayliss, A., Blackwell, P. G., Boswijk, G., Bronk Ramsey, C., Pearson, C., Petchey, F., Reimer, P., Reimer, R. and Wacker, L.: SHCal20 Southern Hemisphere Calibration, 0–55,000 Years cal BP, Radiocarbon, 62(4), 759–778, doi:10.1017/RDC.2020.59, 2020.

Hopmans, E. C., Weijers, J. W. H., Schefuß, E., Herfort, L., Sinninghe Damsté, J. S. and Schouten, S.: Variability in the Benguela Current upwelling system over the past 70,000 years, Earth and Planetary Science Letters, 224(1–2), 107–116, doi:10.1016/j.epsl.2004.05.012, 2004.

Huss, M. and Farinotti, D.: A high-resolution bedrock map for the Antarctic Peninsula, The Cryosphere, 8(4), 1261–1273, doi:10.5194/tc-8-1261-2014, 2014.

Ingólfsson, Ó., Hjort, C. and Humlum, O.: Glacial and Climate History of the Antarctic Peninsula since the Last Glacial Maximum, Arctic, Antarctic, and Alpine Research, 35(2), 175–186, doi:10.1657/1523-0430(2003)035[0175:GACHOT]2.0.CO;2, 2003.

IPCC: Summary for Policymakers, in Climate Change 2021_ The Physical Science Basis. Contribution of working Group I to the Sixth Assessment Report of the Intergovernmental Panel on Climate Change, edited by V. Masson-Delmotte, P. Zhai, H.-O. Pörtner, D. Roberts, J. Skea, P. R. Shukla, A. Pirani, W. Moufouma-Okia,

https://doi.org/10.5194/egusphere-2022-804
Preprint. Discussion started: 24 August 2022

C. Péan, R. Pidcock, S. Connors, J. B. R. Matthews, Y. Chen, X. Zhou, M. I. Gomis, E. Lonnoy, T. Maycock, M. Tignor, and T. Waterfield, p. 32, Cambridge University Press., 2021.

Jones, R. S., Johnson, J. S., Lin, Y., Mackintosh, A. N., Sefton, J. P., Smith, J. A., Thomas, E. R. and Whitehouse, P. L.: Stability of the Antarctic Ice Sheet during the pre-industrial Holocene, Nature Reviews Earth & Environment, doi:10.1038/s43017-022-00309-5, 2022.

Jouzel, J., Vaikmae, R., Petit, J. R., Martin, M., Duclos, Y., Stievenard, M., Lorius, C., Toots, M., Mélières, M. A., Burckle, L. H., Barkov, N. I. and Kotlyakov, V. M.: The two-step shape and timing of the last deglaciation in Antarctica, Climate Dynamics, 11(3), 151–161, doi:10.1007/BF00223498, 1995.

Kalanetra, K. M., Bano, N. and Hollibaugh, J. T.: Ammonia-oxidizing Archaea in the Arctic Ocean and Antarctic coastal waters, Environmental Microbiology, 11(9), 2434–2445, doi:10.1111/j.1462-2920.2009.01974.x, 2009.

Kim, D., Kim, D. Y., Kim, Y. J., Kang, Y. C. and Shim, J.: Downward fluxes of biogenic material in Bransfield Strait, Antarctica, Antarctic Science, 16(3), 227–237, doi:10.1017/S0954102004002032, 2004.

Kim, J.-H., Crosta, X., Willmott, V., Renssen, H., Bonnin, J., Helmke, P., Schouten, S. and Sinninghe Damsté, J. S.: Holocene subsurface temperature variability in the eastern Antarctic continental margin, Geophysical Research Letters, 39(6), doi:10.1029/2012GL051157, 2012.

Klunder, M. B., Laan, P., De Baar, H. J. W., Middag, R., Neven, I. and Van Ooijen, J.: Dissolved Fe across the Weddell Sea and Drake Passage: impact of DFe on nutrient uptake, Biogeosciences, 11(3), 651–669, doi:10.5194/bg-11-651-2014, 2014.

Lamping, N., Müller, J., Esper, O., Hillenbrand, C., Smith, J. A. and Kuhn, G.: Highly branched isoprenoids reveal onset of deglaciation followed by dynamic sea-ice conditions in the western Amundsen Sea, Antarctica, Quaternary Science Reviews, 228, 106103, doi:10.1016/j.quascirev.2019.106103, 2020.

Lamping, N., Müller, J., Hefter, J., Mollenhauer, G., Haas, C., Shi, X., Vorrath, M.-E., Lohmann, G. and Hillenbrand, C.-D.: Evaluation of lipid biomarkers as proxies for sea ice and ocean temperatures along the Antarctic continental margin, Climate of the Past, 17(5), 2305–2326, doi:10.5194/cp-17-2305-2021, 2021.

Lamy, F.: The expedition PS97 of the research vessel POLARSTERN to the Drake Passage in 2016, Reports on Polar and Marine Research, 7'01, 1–571, doi:10.2312/BzPM_0702_2016, 2016.

Lamy, F., Kaiser, J., Arz, H. W., Hebbeln, D., Ninnemann, U., Timm, O., Timmermann, A. and Toggweiler, J. R.: Modulation of the bipolar seesaw in the Southeast Pacific during Termination 1, Earth and Planetary Science Letters, 259(3–4), 400–413, doi:10.1016/j.epsl.2007.04.040, 2007.

Laskar, J., Robutel, P., Joutel, F., Gastineau, M., Correia, A. C. M. and Levrard, B.: A long-term numerical

https://doi.org/10.5194/egusphere-2022-804
Preprint. Discussion started: 24 August 2022

solution for the insolation quantities of the Earth, Astronomy & Astrophysics, 428(1), 261–285, doi:10.1051/0004-6361:20041335, 2004.

Liu, R., Han, Z., Zhao, J., Zhang, H., Li, D., Ren, J., Pan, J. and Zhang, H.: Distribution and source of glycerol dialkyl glycerol tetraethers (GDGTs) and the applicability of GDGT-based temperature proxies in surface sediments of Prydz Bay, East Antarctica, Polar Research, 39, doi:10.33265/polar.v39.3557, 2020.

Lü, X., Liu, X. L., Elling, F. J., Yang, H., Xie, S., Song, J., Li, X., Yuan, H., Li, N. and Hinrichs, K. U.: Hydroxylated isoprenoid GDGTs in Chinese coastal seas and their potential as a paleotemperature proxy for mid-to-low latitude marginal seas, Organic Geochemistry, 89–90, 31–43, doi:10.1016/j.orggeochem.2015.10.004, 2015.

Massé, G., Belt, S. T., Crosta, X., Schmidt, S., Snape, I., Thomas, D. N. and Rowland, S. J.: Highly branched isoprenoids as proxies for variable sea ice conditions in the Southern Ocean, Antarctic Science, 23(05), 487–498, doi:10.1017/S0954102011000381, 2011.

Meijers, A. J. S., Meredith, M. P., Abrahamsen, E. P., Morales Maqueda, M. A., Jones, D. C. and Naveira Garabato, A. C.: Wind-driven export of Weddell Sea slope water, Journal of Geophysical Research: Oceans, 121(10), 7530–7546, doi:10.1002/2016JC011757, 2016.

Meredith, M. P., Falk, U., Bers, A. V., Mackensen, A., Schloss, I. R., Barlett, E. R., Jerosch, K., Busso, A. S. and Abele, D.: Anatomy of a glacial meltwater discharge event in an Antarctic cove, Philosophical Transactions of the Royal Society A: Mathematical, Physical and Engineering Sciences, 376(2122), doi:10.1098/rsta.2017.0163, 2018.

Miles, M. W., Andresen, C. S. and Dylmer, C. V.: Evidence for extreme export of Arctic sea ice leading the abrupt onset of the Little Ice Age, Science Advances, 6(38), doi:10.1126/sciadv.aba4320, 2020.

Milliken, K. T., Anderson, J. B., Wellner, J. S., Bohaty, S. M. and Manley, P. L.: High-resolution Holocene climate record from Maxwell Bay, South Shetland Islands, Antarctica, Geological Society of America Bulletin, 121(11–12), 1711–1725, doi:10.1130/B26478.1, 2009.

Minzoni, R. T., Anderson, J. B., Fernandez, R. and Wellner, J. S.: Marine record of Holocene climate, ocean, and cryosphere interactions: Herbert Sound, James Ross Island, Antarctica, Quaternary Science Reviews, 129, 239–259, doi:10.1016/j.quascirev.2015.09.009, 2015.

Moffat, C. and Meredith, M.: Shelf-ocean exchange and hydrography west of the Antarctic Peninsula: A review, Philosophical Transactions of the Royal Society A: Mathematical, Physical and Engineering Sciences, 376(2122), doi:10.1098/rsta.2017.0164, 2018.

Mollenhauer, G., Grotheer, H., Gentz, T., Bonk, E. and Hefter, J.: Standard operation procedures and

https://doi.org/10.5194/egusphere-2022-804
Preprint. Discussion started: 24 August 2022

performance of the MICADAS radiocarbon laboratory at Alfred Wegener Institute (AWI), Germany, Nuclear Instruments and Methods in Physics Research Section B: Beam Interactions with Materials and Atoms, 496, 45–51, doi:10.1016/j.nimb.2021.03.016, 2021.

Morigi, C., Capotondi, L., Giglio, F., Langone, L., Brilli, M., Turi, B. and Ravaioli, M.: A possible record of the Younger Dryas event in deep-sea sediments of the Southern Ocean (Pacific sector), in Palaeogeography, Palaeoclimatology, Palaeoecology, vol. 198, pp. 265–278, Elsevier B.V., 2003.

Mortlock, R. A. and Froelich, P. N.: A simple method for the rapid determination of biogenic opal in pelagic marine sediments, Deep Sea Research Part A, Oceanographic Research Papers, 36(9), 1415–1426, doi:10.1016/0198-0149(89)90092-7, 1989.

Müller, J., Wagner, A., Fahl, K., Stein, R., Prange, M. and Lohmann, G.: Towards quantitative sea ice reconstructions in the northern North Atlantic: A combined biomarker and numerical modelling approach, Earth and Planetary Science Letters, 306(3–4), 137–148, doi:10.1016/J.EPSL.2011.04.011, 2011.

Müller, P. J. and Schneider, R.: An automated leaching method for the determination of opal in sediments and particulate matter, Deep-Sea Research Part I, 40(3), 425–444, doi:https://doi.org/10.1016/0967-0637(93)90140-X, 1993.

Mulvaney, R., Abram, N. J., Hindmarsh, R. C. A., Arrowsmith, C., Fleet, L., Triest, J., Sime, L. C., Alemany, O. and Foord, S.: Recent Antarctic Peninsula warming relative to Holocene climate and ice-shelf history, Nature, 489(7414), 141–144, doi:10.1038/nature11391, 2012.

Nicholls, K. W., Østerhus, S., Makinson, K., Gammelsrød, T. and Fahrbach, E.: Ice-ocean processes over the continental shelf of the southern Weddell Sea, Antarctica: A review, Reviews of Geophysics, 47(3), RG3003, doi:10.1029/2007RG000250, 2009.

Ó Cofaigh, C., Davies, B. J., Livingstone, S. J., Smith, J. A., Johnson, J. S., Hocking, E. P., Hodgson, D. A., Anderson, J. B., Bentley, M. J., Canals, M., Domack, E., Dowdeswell, J. A., Evans, J., Glasser, N. F., Hillenbrand, C.-D., Larter, R. D., Roberts, S. J. and Simms, A. R.: Reconstruction of ice-sheet changes in the Antarctic Peninsula since the Last Glacial Maximum, Quaternary Science Reviews, 100, 87–110, doi:10.1016/j.quascirev.2014.06.023, 2014.

Oksanen, J., Blanchet, F. G., Kindt, R., Legendre, P., Minchin, P. R., O´Hara, R. B., Simpson, G. L., Solymos, P., Stevens, M. H. H. and Wagner, H.: Vegan: Community Ecology Package (R Package Version 2.0-3), 2012.

Parkinson, C. L.: Search for the Little Ice Age in Southern Ocean Sea-Ice Records, Annals of Glaciology, 14, 221–225, doi:10.3189/S0260305500008624, 1990.

Parkinson, C. L. and Cavalieri, D. J.: Antarctic sea ice variability and trends, 1979–2010, The Cryosphere, 6, 871–880, doi:10.5194/tc-6-871-2012, 2012.

Pedro, J. B., Bostock, H. C., Bitz, C. M., He, F., Vandergoes, M. J., Steig, E. J., Chase, B. M., Krause, C. E., Rasmussen, S. O., Markle, B. R. and Cortese, G.: The spatial extent and dynamics of the Antarctic Cold Reversal, Nature Geoscience, 9(1), 51–55, doi:10.1038/ngeo2580, 2016.

QGIS, D. T.: QGIS Geographic Information System, [online] Available from: http://qgis.osgeo.org, 2018.

R Core Team: R: a Language and Environment for Statistical Computing, R Foundation for Statistical computing, Vienna., 2012.

Reynolds, R. W., Rayner, N. A., Smith, T. M., Stokes, D. C., Wang, W., Reynolds, R. W., Rayner, N. A., Smith, T. M., Stokes, D. C. and Wang, W.: An Improved In Situ and Satellite SST Analysis for Climate, Journal of Climate, 15(13), 1609–1625, doi:10.1175/1520-0442(2002)015<1609:AIISAS>2.0.CO;2, 2002.

Reynolds, R. W., Smith, T. M., Liu, C., Chelton, D. B., Casey, K. S., Schlax, M. G., Reynolds, R. W., Smith, T. M., Liu, C., Chelton, D. B., Casey, K. S. and Schlax, M. G.: Daily High-Resolution-Blended Analyses for Sea Surface Temperature, Journal of Climate, 20(22), 5473–5496, doi:10.1175/2007JCLI1824.1, 2007.

Rignot, E., Mouginot, J., Scheuchl, B., van den Broeke, M., van Wessem, M. J. and Morlighem, M.: Four decades of Antarctic Ice Sheet mass balance from 1979–2017, Proceedings of the National Academy of Sciences, 116(4), 1095–1103, doi:10.1073/pnas.1812883116, 2019.

Roche, D. M., Crosta, X. and Renssen, H.: Evaluating Southern Ocean sea-ice for the Last Glacial Maximum and pre-industrial climates: PMIP-2 models and data evidence, Quaternary Science Reviews, 56, 99–106, doi:10.1016/j.quascirev.2012.09.020, 2012.

Ronge, T. A., Lippold, J., Geibert, W., Jaccard, S. L., Mieruch-Schnülle, S., Süfke, F. and Tiedemann, R.: Deglacial patterns of South Pacific overturning inferred from 231Pa and 230Th, Scientific Reports, 11(1), doi:10.1038/s41598-021-00111-1, 2021.

Roseby, Z. A., Smith, J. A., Hillenbrand, C.-D., Cartigny, M. J. B., Rosenheim, B. E., Hogan, K. A., Allen, C. S., Leventer, A., Kuhn, G., Ehrmann, W. and Larter, R. D.: History of Anvers-Hugo Trough, western Antarctic Peninsula shelf, since the Last Glacial Maximum. Part I: Deglacial history based on new sedimentological and chronological data, Quaternary Science Reviews, 291, 107590, doi:10.1016/j.quascirev.2022.107590, 2022.

Sangrà, P., Gordo, C., Hernández-Arencibia, M., Marrero-Díaz, A., Rodríguez-Santana, A., Stegner, A., Martínez-Marrero, A., Pelegrí, J. L. and Pichon, T.: The Bransfield current system, Deep Sea Research Part I: Oceanographic Research Papers, 58(4), 390–402, doi:10.1016/J.DSR.2011.01.011, 2011.

Sangrà, P., Stegner, A., Hernández-Arencibia, M., Marrero-Díaz, Á., Salinas, C., Aguiar-González, B., Henríquez-Pastene, C. and Mouriño-Carballido, B.: The Bransfield Gravity Current, Deep-Sea Research Part I:

https://doi.org/10.5194/egusphere-2022-804
Preprint. Discussion started: 24 August 2022

Oceanographic Research Papers, 119(November 2016), 1–15, doi:10.1016/j.dsr.2016.11.003, 2017.

Scherer, R. P.: A new method for the determination of absolute abundance of diatoms and other silt-sized sedimentary particles, Journal of Paleolimnology, 12(2), 171–179, doi:10.1007/BF00678093, 1994.

Schlüter, M. and Rickert, D.: Effect of pH on the measurement of biogenic silica, Marine Chemistry, 63(1–2), 81–92, doi:10.1016/S0304-4203(98)00052-8, 1998.

Schofield, O., Brown, M., Kohut, J., Nardelli, S., Saba, G., Waite, N. and Ducklow, H.: Changes in the upper ocean mixed layer and phytoplankton productivity along the West Antarctic Peninsula, Philosophical Transactions of the Royal Society A: Mathematical, Physical and Engineering Sciences, 376(2122), doi:10.1098/rsta.2017.0173, 2018.

Schrader, H. and Gersonde, R.: Diatoms and silicoflagellates, in Micropaleontological Methods and Techniques - An Excercise on an Eight Meter Section of the Lower Pliocene of Capo Rossello, Sicily, Utrecht Micropaleontological Bulletins, vol. 17, edited by W. J. Zachariasse, W. R. Riedel, A. Sanfilippo, R. R. Schmidt, M. J. Brolsma, H. J. Schrader, R. Gersonde, M. M. Drooger, and J. A. Broekman, pp. 129–176., 1978.

Shevenell, A. E., Ingalls, A. E., Domack, E. W. and Kelly, C.: Holocene Southern Ocean surface temperature variability west of the Antarctic Peninsula, Nature, 470(7333), 250–254, doi:10.1038/nature09751, 2011.

Simms, A. R., Bentley, M. J., Simkins, L. M., Zurbuchen, J., Reynolds, L. C., DeWitt, R. and Thomas, E. R.: Evidence for a “Little Ice Age” glacial advance within the Antarctic Peninsula – Examples from glacially-overrun raised beaches, Quaternary Science Reviews, 271, 107195, doi:10.1016/j.quascirev.2021.107195, 2021.

Simpson, G. L. and Oksanen, J.: Analogue: Analogue Matching and Modern Analogue Technique Transfer Function Models. R Package Version 0.8-2, 2012.

Sjunneskog, C. and Taylor, F.: Postglacial marine diatom record of the Palmer Deep, Antarctic Peninsula (ODP Leg 178, Site 1098) 1. Total diatom abundance, Paleoceanography, 17(3), PAL 4-1-PAL 4-8, doi:10.1029/2000PA000563, 2002.

Smetacek, V., Assmy, P. and Henjes, J.: The role of grazing in structuring Southern Ocean pelagic ecosystems and biogeochemical cycles, Antarctic Science, 16(4), 541–558, doi:10.1017/S0954102004002317, 2004.

Smith, J. A., Graham, A. G. C., Post, A. L., Hillenbrand, C.-D., Bart, P. J. and Powell, R. D.: The marine geological imprint of Antarctic ice shelves, Nature Communications, 10(1), 5635, doi:10.1038/s41467-019-13496-5, 2019.

Stenni, B., Masson-Delmotte, V., Johnsen, S., Jouzel, J., Longinelli, A., Monnin, E., Röthlisberger, R. and Selmo, E.: An Oceanic Cold Reversal During the Last Deglaciation, Science, 293(5537), 2074–2077, doi:10.1126/science.1059702, 2001.

https://doi.org/10.5194/egusphere-2022-804
Preprint. Discussion started: 24 August 2022

Stuiver, M., Reimer, P. J. and Reimer, R. W.: Calib 7.1, [online] Available from: http://calib.org/ (Accessed 20 November 2021), 2018.

Thomas, Allen, Etourneau, King, Severi, Winton, Mueller, Crosta and Peck: Antarctic Sea Ice Proxies from Marine and Ice Core Archives Suitable for Reconstructing Sea Ice over the past 2000 Years, Geosciences, 9(12), 506, doi:10.3390/geosciences9120506, 2019.

Timmermann, A., Okumura, Y., An, S.-I., Clement, A., Dong, B., Guilyardi, E., Hu, A., Jungclaus, J. H., Renold, M., Stocker, T. F., Stouffer, R. J., Sutton, R., Xie, S.-P. and Yin, J.: The Influence of a Weakening of the Atlantic Meridional Overturning Circulation on ENSO, Journal of Climate, 20(19), 4899–4919, doi:10.1175/JCLI4283.1, 2007.

Totten, R. L., Fonseca, A. N. R., Wellner, J. S., Munoz, Y. P., Anderson, J. B., Tobin, T. S. and Lehrmann, A. A.: Oceanographic and climatic influences on Trooz Glacier, Antarctica during the Holocene, Quaternary Science Reviews, 276, 107279, doi:10.1016/j.quascirev.2021.107279, 2022.

Turner, J., Orr, A., Gudmundsson, G. H., Jenkins, A., Bingham, R. G., Hillenbrand, C.-D. and Bracegirdle, T. J.: Atmosphere-ocean-ice interactions in the Amundsen Sea Embayment, West Antarctica, Reviews of Geophysics, 55(1), 235–276, doi:10.1002/2016RG000532, 2017.

Vancoppenolle, M., Meiners, K. M., Michel, C., Bopp, L., Brabant, F., Carnat, G., Delille, B., Lannuzel, D., Madec, G., Moreau, S., Tison, J. L. and van der Merwe, P.: Role of sea ice in global biogeochemical cycles: Emerging views and challenges, Quaternary Science Reviews, 79, 207–230, doi:10.1016/j.quascirev.2013.04.011, 2013.

Vaughan, D. G., Marshall, G. J., Connolley, W. M., Parkinson, C., Mulvaney, R., Hodgson, D. A., King, J. C., Pudsey, C. J. and Turner, J.: Recent Rapid Regional Climate Warming on the Antarctic Peninsula, Climatic Change, 60(3), 243–274, doi:10.1023/A:1026021217991, 2003.

Vernet, M., Martinson, D., Iannuzzi, R., Stammerjohn, S., Kozlowski, W., Sines, K., Smith, R. and Garibotti, I.: Primary production within the sea-ice zone west of the Antarctic Peninsula: I—Sea ice, summer mixed layer, and irradiance, Deep Sea Research Part II: Topical Studies in Oceanography, 55(18–19), 2068–2085, doi:10.1016/j.dsr2.2008.05.021, 2008.

Vorrath, M.-E., Müller, J., Esper, O., Mollenhauer, G., Haas, C., Schefuß, E. and Fahl, K.: Highly branched isoprenoids for Southern Ocean sea ice reconstructions: a pilot study from the Western Antarctic Peninsula, Biogeosciences, 16(15), 2961–2981, doi:10.5194/bg-16-2961-2019, 2019.

Vorrath, M.-E., Müller, J., Rebolledo, L., Cárdenas, P., Shi, X., Esper, O., Opel, T., Geibert, W., Muñoz, P., Haas, C., Kuhn, G., Lange, C. B., Lohmann, G. and Mollenhauer, G.: Sea ice dynamics in the Bransfield Strait,

https://doi.org/10.5194/egusphere-2022-804
Preprint. Discussion started: 24 August 2022

Antarctic Peninsula, during the past 240 years: a multi-proxy intercomparison study, Climate of the Past, 16(6), 2459–2483, doi:10.5194/cp-16-2459-2020, 2020.

WAIS Divide Project Members: Onset of deglacial warming in West Antarctica driven by local orbital forcing, Nature, 500(7463), 440–444, doi:10.1038/nature12376, 2013.

WAIS Divide Project Members: Precise interpolar phasing of abrupt climate change during the last ice age, Nature, 520(7549), 661–665, doi:10.1038/nature14401, 2015.

Warnock, J. P. and Scherer, R. P.: A revised method for determining the absolute abundance of diatoms, Journal of Paleolimnology, 53(1), 157–163, doi:10.1007/s10933-014-9808-0, 2014.

Wefer, G., Fischer, G., Füetterer, D. and Gersonde, R.: Seasonal particle flux in the Bransfield Strait, Antartica, Deep Sea Research Part A. Oceanographic Research Papers, 35(6), 891–898, doi:10.1016/0198-0149(88)90066-0, 1988.

Wu, S., Kuhn, G., Diekmann, B., Lembke-Jene, L., Tiedemann, R., Zheng, X., Ehrhardt, S., Arz, H. W. and Lamy, F.: Surface sediment characteristics related to provenance and ocean circulation in the Drake Passage sector of the Southern Ocean, Deep Sea Research Part I: Oceanographic Research Papers, 154, 103135, doi:10.1016/j.dsr.2019.103135, 2019.

Zhou, M., Niiler, P. P. and Hu, J. H.: Surface currents in the Bransfield and Gerlache Straits, Antarctica, Deep-Sea Research Part I: Oceanographic Research Papers, 49(2), 267–280, doi:10.1016/S0967-0637(01)00062-0, 2002.

Zwally, H. J., Comiso, J. C., Parkinson, C. L., Cavalieri, D. J. and Gloersen, P.: Variability of Antarctic sea ice 1979–1998, Journal of Geophysical Research, 107(C5), 3041, doi:10.1029/2000JC000733, 2002.

https://doi.org/10.5194/egusphere-2022-804
Preprint. Discussion started: 24 August 2022

Figures

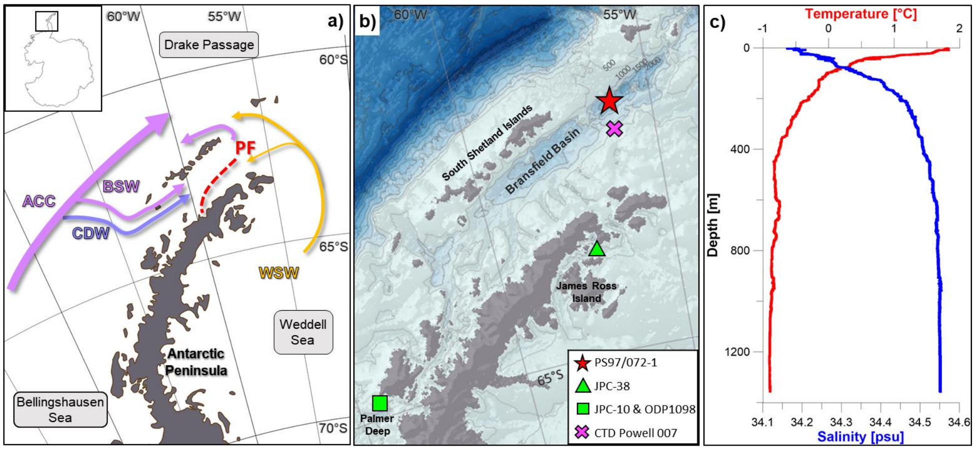

Figure 1: a) Overview map with modern oceanography in the study area (Hofmann et al., 1996; Sangrà et al., 2011)**. ACC = Antarctic Circumpolar Current, BSW = Bellingshausen Sea Water, CDW = Circumpolar Deep Water, WSW = Weddell Sea Water, and PF = Peninsula Front. b) Bathymetric features in the Bransfield Strait with the location of sediment core PS97/072-1 (red star) and other sediment records discussed in the text (green), and the CTD station (purple cross) where c) the vertical profile of ocean temperature and salinity (cruise POWELL2020, CTD 007 (62°09.075'S, 56°37.09'W) from 27.01.2020) shows a clear stratification of the upper 100 m of the water column. It indicates that surface waters are dominated by the BSW, while the basin is filled with WSW water. Maps were done with QGIS 3.0** (QGIS, 2018) **and the bathymetry was taken from GEBCO_14 from 2015.**

https://doi.org/10.5194/egusphere-2022-804
Preprint. Discussion started: 24 August 2022

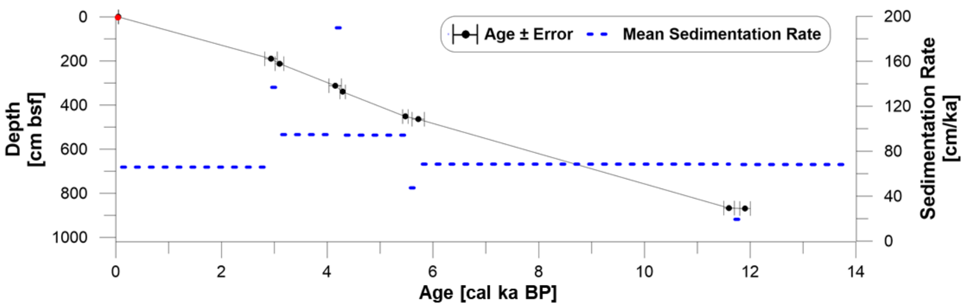

Figure 2: Age-depth model for sediment core PS97/72-1 based on eight ^{14}C dated calcite samples (black) with error bars and mean sedimentation rates (cm/ka, dashed blue line). The core top age (red) was estimated as 0.05 ka BP from matching with the ^{210}Pb-dated multicore PS97/072-2 (Vorrath et al., 2019; see supplement section 2)**.**

https://doi.org/10.5194/egusphere-2022-804
Preprint. Discussion started: 24 August 2022

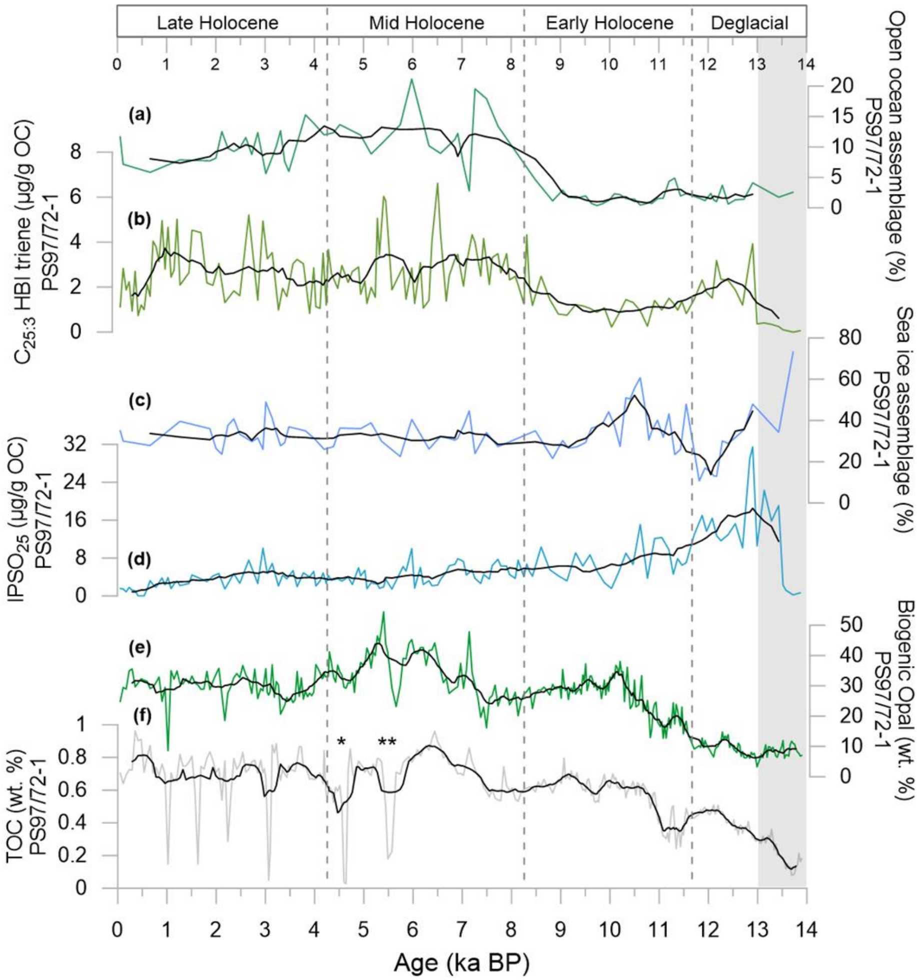

Figure 3: Overview of organic geochemical parameters and main diatom assemblages determined in sediment core PS97/72-1 used to characterize the environmental setting over the past 14 ka BP. a) open ocean diatom assemblage, b) $C_{25:3}$ HBI triene, c) sea ice diatom assemblage, d) $IPSO_{25}$, e) biogenic opal and f) TOC contents. Asterisks in f) mark layers of volcanic ash, where ** can be linked to a tephra layer in a sediment core from the Bransfield Strait at 5.5 ka BP (Heroy et al., 2008). **Grey shaded interval refers to the ACR.**

https://doi.org/10.5194/egusphere-2022-804
Preprint. Discussion started: 24 August 2022

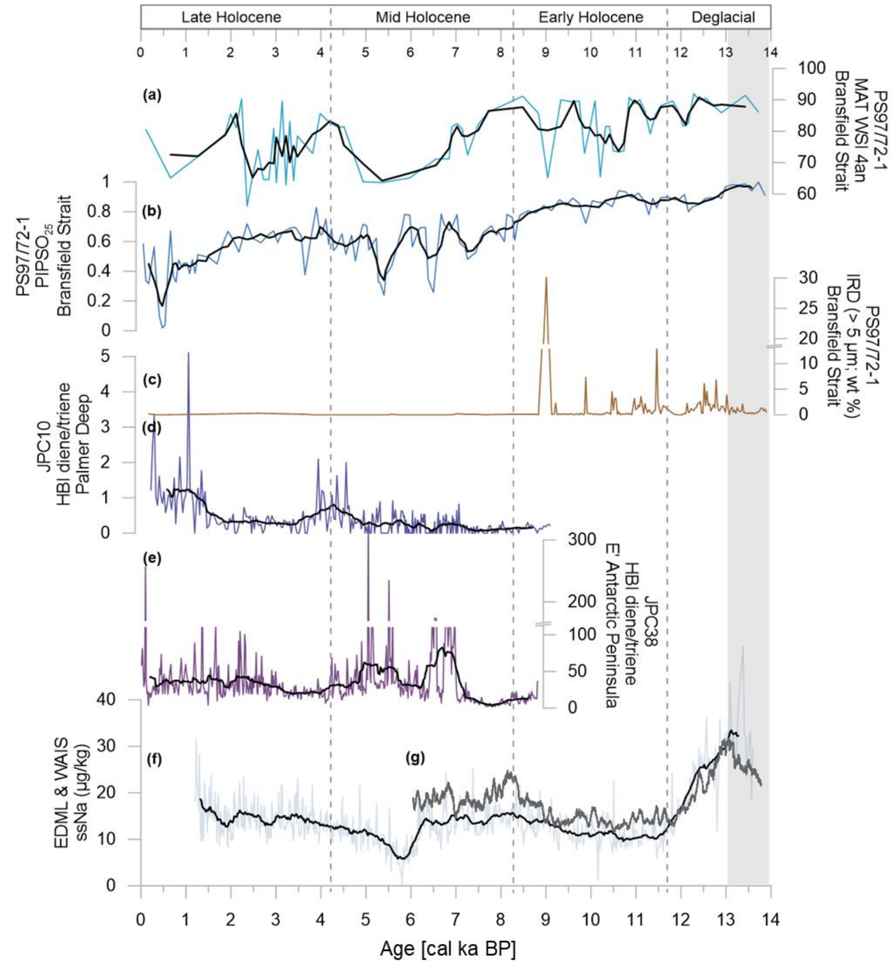

Figure 4: Sea ice related proxies in sediment core PS97/72-1 with a) the diatom based WSI, b) the sea ice index PIPSO$_{25}$, and c) ice rafted debris (IRD). For comparison: the HBI diene/triene ratio of sediment core d) JPC10 from the Palmer Deep station (Etourneau et al., 2013) **and e) JPC38 at the East Antarctic Peninsula** (Barbara et al., 2016)**. ssNa records of f) the EDML ice core** (Fischer et al., 2007) **and g) the WAIS ice core** (WAIS Divide Project Members, 2015)**. Grey shaded interval refers to the ACR.**

https://doi.org/10.5194/egusphere-2022-804
Preprint. Discussion started: 24 August 2022

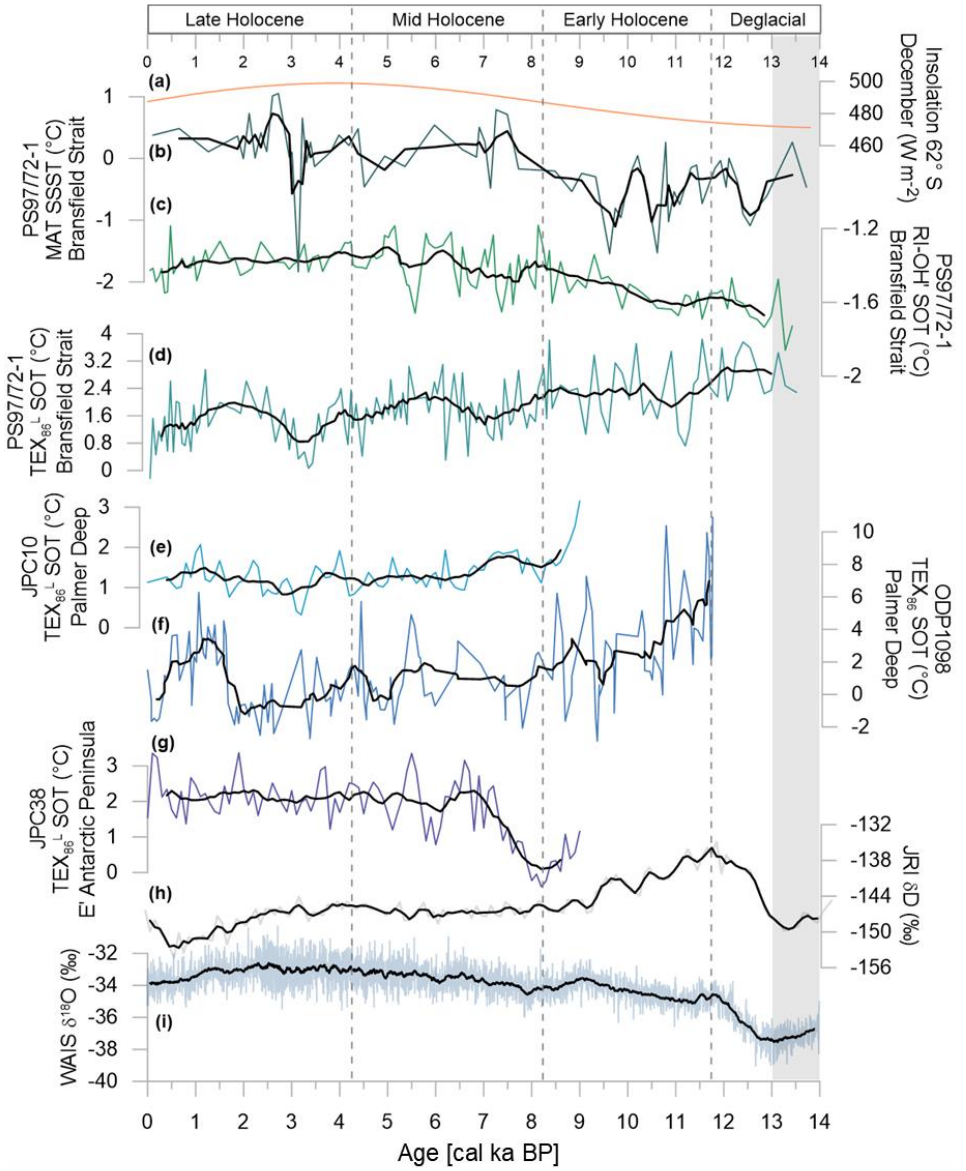

Figure 5: A comparison of a) December insolation (Laskar et al., 2004)**, b) diatom-based SSST, c) RI-OH'-derived SOT, d) TEX_{86}^{L}-SOT of sediment core PS97/72-1, and temperature reconstructions e) TEX_{86}^{L} from JPC10, Palmer Deep, d) TEX_{86} from ODP1098, Palmer Deep, e) TEX_{86}^{L} from JPC38, East Antarctic Peninsula, and ice core stable isotope records of h) JRI** (Mulvaney et al., 2012) **and i) WAIS Divide** (WAIS Divide Project Members, 2013)**.**